Motion-Induced Blindness as a Noisy Excitable System

Mikhail Katkov, Alexander Cooperman✡, Noya Meital-Kfir, and Dov Sagi*

Department of Brain Sciences, The Weizmann Institute of Science, Rehovot, Israel

✡*This article is dedicated to the memory of Dr. Alexander Cooperman (1930-2019) for his tremendous contribution and initiative.* Alex Cooperman first envisioned the possibility of describing MIB as a dynamical system, he carried out many pilot studies but did not have enough time to complete his work. *An earlier version of this work was presented at the 2015 meeting of the Israeli Society for Neuroscience.*

*Corresponding author: mikhail.katkov@gmail.com

Abstract

Perceptual disappearance of a salient target induced by a moving texture mask (MIB: Motion Induced Blindness) is a striking effect that is currently poorly understood. Here we investigated whether the mechanisms underlying MIB qualify as an excitable system. Excitable systems exhibit fast switches from one state to another (e.g., visible/invisible) induced by an above threshold perturbation and stimulus-independent dynamics, followed by a refractory period. In the experiments, disappearance was induced by masks consisting of slowly rotating radial bars with a gap at the target location, leading to periodic perturbation of the visual field around the target (a bright parafoveal spot).

Only when the bars passed around the target location did they induce an abrupt target disappearance, independent of the rotation speed (up to 90%, depending on the condition, ~0% without bars), pointing to locality. The distribution of invisible periods is well described as the sum of two random variables: Gamma and Gaussian distributed. As expected from excitable systems, the disappearance time was not affected by additional bars crossing the target during invisibility. After the target reappeared, it stayed for at least 0.5-2 sec (the refractory period).

Overall, slowly moving bars are very good inducers of perceptual disappearance when the targets are visible, whereas they hardly affect an invisible target. The periods of invisibility lasted a few seconds, showing little dependence on the mask configuration. Therefore, the mechanisms governing MIB represent an example of an excitable system where the transition to the invisible state is induced by the mask, with the dynamics that follow determined mostly by the internal network properties. The implementation of such systems usually requires two components with substantially different time scales, such as adaptation and inhibition.

Introduction:

Motion-Induced Blindness (MIB) is a striking phenomenon where a moving mask suppresses the perception of a physically present static target (Bonneh et al., 2001). MIB disappearances are an all-or-none phenomenon and can last up to several seconds, even with a high-contrast target located near fixation (Bonneh et al., 2014). Furthermore, invisibility can be perturbed by a similar visible cue flashed at the target neighborhood (Meital-Kfir & Sagi, 2018), indicating that the neuronal networks involved in invisibility preserve the sensitivity. Despite the detailed experimental exploration of MIB, the underlying mechanism remains unknown. Here, we consider the application of the theory of dynamical systems, which was found useful in describing bistable phenomena.

MIB, with the corresponding spontaneous transition between seen and not-seen states, is often treated as a bistable phenomenon (Bonneh et al., 2014; Devyatko et al., 2017; Hsu et al., 2006; Jaworska & Lages, 2014). MIB was found to be affected by stimulation parameters in a way similar to that of binocular rivalry; the two phenomena show a highly correlated pattern of perceptual transitions across individuals (Carter & Pettigrew, 2003). Others point to large individual differences in MIB measurements as a modeling challenge, arguing that "normative models of MIB may not be practical" (Sparrow et al., 2017). One interesting approach to describe bistable phenomena is based on modeling a stable percept as an attractor state – the persistent activity of a group of neurons (Braun & Mattia, 2010; Cao et al., 2021). The irregular switching between percepts in this model is governed by the intrinsic noise, which drives the network state between the two attractors.

An important difference between MIB and other bistable phenomena, such as binocular rivalry, lies in the number of stable states. Whereas in bistable phenomena two percepts may equally last for prolonged periods, in MIB the invisibility state is unstable, exhibiting a transient behavior. In dynamical systems theory, such behavior characterizes excitable systems. For example, consider a spiking neuron. In the absence of a strong input, the neuron is in a resting state – small input fluctuations lead to small fluctuations in the membrane potential, tracking the input frequency. However, when the input exceeds a threshold level, the neuron exhibits a spiking behavior. Once a spike is initiated, the membrane potential changes substantially and is weakly dependent on the input. The temporal profile of the spike is prototypical and largely depends on the properties of the neuron, but not on the properties of the input. When the spiking activity ends, there is a measurable refractory period during which the neuron cannot emit spikes.

Stochastic resonance is a notable feature in the presence of noise, in both bistable and excitable systems (Duki & Taye, 2018; Lindner et al., 2004; Longtin & Chialvo, 1998; Muratov et al., 2005; Versteegen et al., 2016; Volkov et al., 2003). In the absence of

noise or external perturbation, the dynamics of a bistable system converge to one of the stable states, whereas an excitable system would converge to its resting state. In the presence of a sufficient amount of noise, a bistable system switches between stable states, whereas an excitable system repeatedly undergoes a large trajectory; each trajectory ends at its resting state. The detailed dynamics underlying these transitions, which depend on the strength of the noise and the properties of the system, can be explored using periodic external stimulation. A stimulation period that is close to the characteristic system time constant is expected to facilitate switching at a stimulation frequency. In contrast, when the stimulation frequency is too high, the system, while in transit toward its stable state, is insensitive to external stimulation and is not expected to be affected by the frequent incoming stimulation. When the stimulation frequency is too low, since intrinsic dynamics is faster than the driving frequency, several switches are possible during a single stimulation period that broadens the response in the frequency domain. Overall, this looks like a noise-assisted resonance – there is a specific noise-dependent frequency of stimulation that leads to optimal switching behavior at a stimulation frequency (Gammaitoni et al., 1998; Muratov et al., 2005).

Here we use periodic stimulation to study the dynamics of MIB, while considering the mask as a driving force. Employing a periodic mask, we expect with the limit of low noise: (1) a minimal, non-zero duration of invisibility, defined by the system dynamics, before the system relaxes to a visible resting state; (2) a refractory period – a minimal visibility time before the target can disappear again; (3) a non-monotonic dependency of mask efficiency (S/N) on the mask period. We have found that roughly half of the observers do not have invisibility periods shorter than 100-200 ms, suggesting that there is a minimum duration of invisibility (see also Meital-Kfir et al., 2016). Visible periods for most people were not shorter than 1-2 sec. Finally, analysis of the signal-to-noise ratio (SNR) in the switching traces shows a non-monotonic dependence on the stimulation frequency. We also show that the distribution of switching times is well described by the sum of two random variables: one is Gamma distributed and the other is Gaussian distributed. We attributed the former variable to the statistical properties of the internal dynamics, whereas the latter variable describes the minimal delay due to neuronal dynamics and jitter in the motor response when reporting a disappearance.

Results:

To efficiently track the dependence of perceptual transitions on a mask structure, we employed masks consisting of discrete, well-defined parts. The mask (Figure 1) consisted of bars rotating around a fixation point (with breaks inserted to avoid physical interference with the target); the number of bars and their speed was varied to control the mask frequency (see the Methods). Note that we report the period of the mask as the minimal time between identical image appearances on the screen.

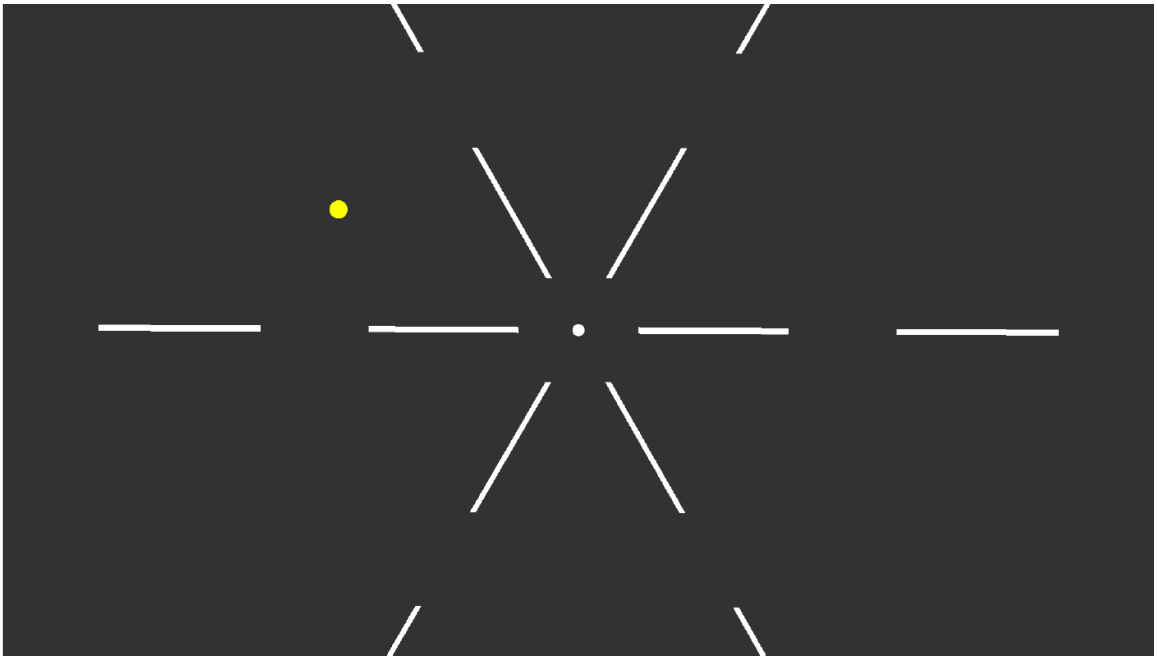

Figure 1 An example of stimuli used in the experiments. A screenshot of stimulus shown on 24" display that was viewed from a distance of 120 cm.

Figure 2 depicts the dependency of the perceptual state on the phase of the mask for two observers. Clearly, the disappearance report (the black lines) lacks a structure for short periods (1 sec) of mask rotation, but it was phase locked for longer periods (4 sec). The results for all observers are shown in the supplementary materials. For the longer rotation period (4 sec), the target was reported as visible during some phases of the stimulation cycle on practically every mask cycle, whereas during other phases, visibility reports were recorded on only 65- 80% of the cycles. This indicates that the moving bars are effective inducers of MIB. In contrast, with the shorter mask period (1 sec), the invisibility reports were uniformly distributed during the stimulation cycle, indicating that the system does not have sufficient time for relaxation from the invisible state. The simple mathematical properties of this mask enable a systematic study of the specific mechanisms governing disappearances. Moreover, at slow rotation speeds, this mask can

be used to study interactions across the boundary of awareness, since for slow presentation periods the time of invisibility is highly predictable.

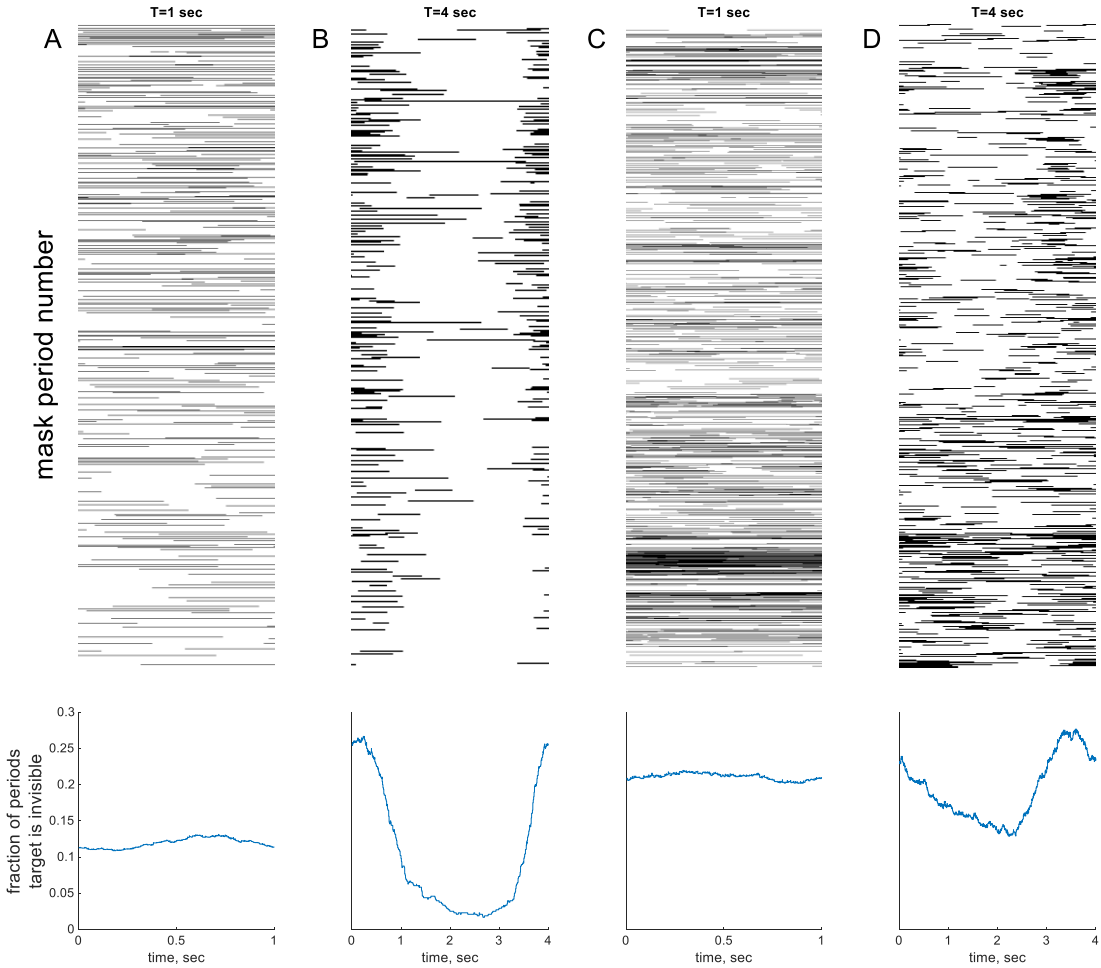

Figure 2. **Examples of disappearance patterns from 2 participants and 2 stimulation frequencies.** Top row: A raster plot of the invisibility reports. The black regions represent moments when the target was reported absent. Consecutive periods of mask rotation are stacked vertically. Bottom row: The disappearance rates of a target as a function of time within one stimulation cycle. (A) and (B) are the results from one human observer for mask periods of 1 sec (A) and 4 sec (B). (C) and (D) the same as (A) and (B) obtained from another human observer. One can observe that the disappearance rate toward the end of the cycle for both observers approaches 25%, indicating the high effectiveness of the mask to induce MIB. In contrast, in the middle of the cycle for slow mask periods (B, D) there are reduced disappearance rates. For example, in (B) the target is practically always visible in the middle of the cycle.

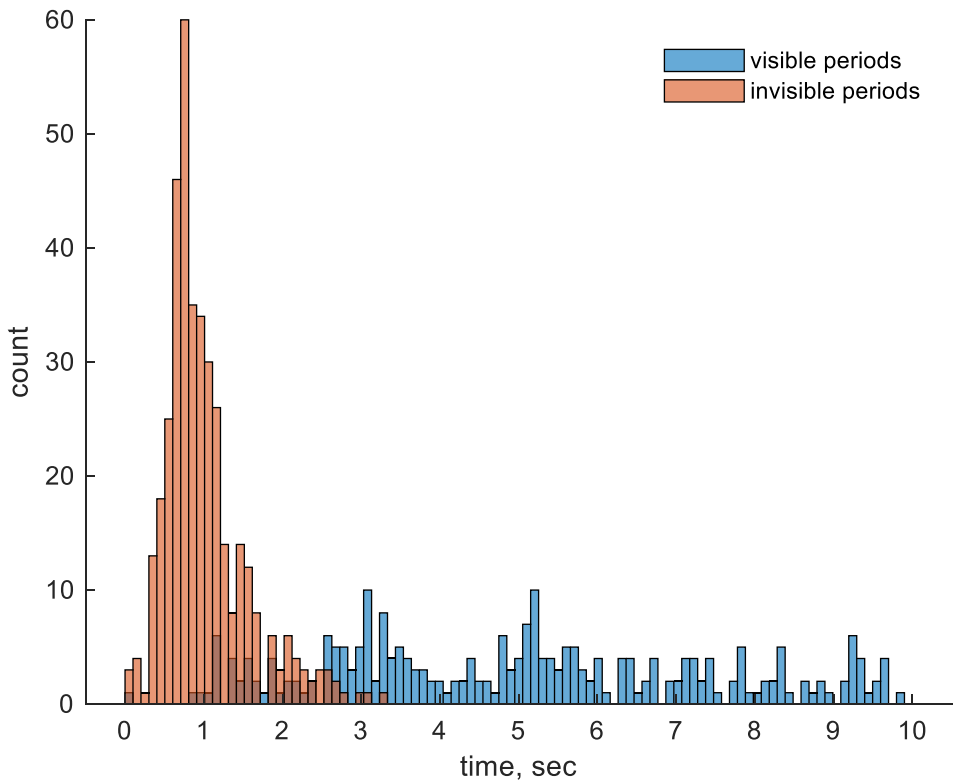

Figure 3. Example of the distributions of visible and invisible periods for one observer and one condition.

To determine whether a refractory period is present, we examined the distribution of visible periods (Figure 3, and Supplementary material). One can see that all visible periods in this example are longer than 1 second. This is not explained by limits on the reporting speed, since there are many invisible periods with shorter durations. Within the context of the current theory, this minimal duration is due to the system's refractory period, that is, the system needs to recover from one invisibility epoch before transitioning to a new invisibility epoch. That is, when the target becomes visible, it will stay visible for some minimum time.

In 140 out of 148 conditions, the distribution of the invisible periods is well described by the sum of gamma distributed and normally distributed random variables, assuming a 5% criterion for the Kolmogorov-Smirnov test. The normally distributed random variable represents the noisy reaction time for pressing and releasing the keyboard space bar, and the average transition time through the excited state back to the resting state (see Table 1, and the supplementary material). One can also observe that the Gaussian distribution parameters are relatively consistent for the same observer in all experimental conditions, probably indicating prototypical dynamics. The gamma distribution parameters are more variable, even within the same observer, possibly indicating the differential effect of the mask. For instance, one can observe that the values of κ (the shape parameter, see Eq.1 in

the Methods) are more consistent in conditions with moving masks than in the static conditions (e.g. Troxler, see the condition details in the Methods). We found that the estimated distributions cannot be rejected using Kolmogorov-Smirnoff statistics, as detailed in the Supplementary material. Overall, considering all the experiments, the fraction of the fitted distributions that can be rejected is within the rejection criterion p-value, indicating that the mixture model provides an excellent description of our data.

	κ	θ	μ	σ	p		κ	θ	μ	σ	p
	O1						O2				
Troxler	0.95	0.66	0.49	0.24	0.68		0.61	0.70	0.29	0.13	1.00
Static mask	0.99	0.47	0.57	0.11	1.00		0.42	0.73	0.29	0.13	0.98
1 sec	1.58	0.97	0.75	0.35	0.04		0.86	0.70	0.43	0.46	0.05
2 sec	1.53	0.95	0.66	0.10	0.17		0.95	0.73	0.38	0.35	0.33
4 sec	1.35	0.28	1.12	0.34	0.77		0.92	0.82	0.36	0.28	0.72
8 sec	1.31	0.79	0.61	0.13	0.22		0.93	0.71	0.44	0.36	0.82
	O3						O4				
Troxler	0.59	0.44	0.37	0.16	0.95		1.15	0.25	0.76	0.16	0.62
Static mask	0.78	0.42	0.44	0.20	0.91		1.07	0.22	0.84	0.21	0.68
1 sec	0.85	0.62	0.47	0.21	0.89		0.84	0.50	0.79	0.28	0.59
2 sec	1.31	0.41	0.48	0.10	0.58		0.91	0.35	0.79	0.10	0.68
4 sec	0.95	0.53	0.49	0.15	0.48		1.22	0.17	0.93	0.19	0.57
8 sec	1.08	0.57	0.54	0.16	0.37		0.01	0.70	1.26	0.40	0.67
	O5						O6				
Troxler	0.38	0.65	0.10	0.09	0.97		0.94	0.28	0.46	0.07	1.00
Static mask	0.80	0.72	0.46	0.22	1.00		0.37	0.15	0.45	0.09	0.95
1 sec	1.05	0.62	0.58	0.11	0.76		0.91	0.50	0.49	0.19	0.95
2 sec	0.87	0.52	0.56	0.17	0.90		0.86	0.50	0.49	0.14	0.99
4 sec	0.94	0.49	0.59	0.19	1.00		0.97	0.38	0.47	0.13	0.93
8 sec	0.99	0.54	0.50	0.11	0.58		0.86	0.39	0.51	0.09	0.22

Table 1. The distribution parameters for the disappearance times. The distributions were assumed to be the sum of two random variables, one normally distributed and one gamma distributed. The symbols κ and θ represent the shape and scale parameters of the gamma distribution; μ and σ are the mean and SD of the normal distribution, respectively. p represents the p-value of the Kolmogorov-Smirnoff goodness of fit. All six observers are shown (3 rows X 2 columns). The highlighted columns show the constant delay before the target reappears, representing a long excursion time (~0.5 sec) in an excitable system until it returns to a stable state. One can see that these times are relatively consistent for the same observer in all experimental conditions, probably indicating prototypical dynamics. The symbol σ probably indicates the jitter in the response. The parameters of the gamma distribution are more variable, even within the same observer, possibly indicating the differential effect of the mask. For instance, one can see that the κ values are more consistent in conditions with a moving mask than in the Troxler or static mask conditions (see the condition details in the Methods).

We have shown, so far, evidence supporting the presence of a refractory period following the invisibility state, and a delay in the dynamics until the system returns to the resting state. Next, we will show the presence of stochastic resonance. Figure 4 shows the signal-to-noise ratio (SNR, see the Methods for details) for each observer for different rotating mask periods. As one can see, for most observers there is a non-monotonic dependence of SNR on the mask frequency, typical for stochastic resonance. One observer shows monotonic dependence, possibly indicating that the resonance is at a higher frequency.

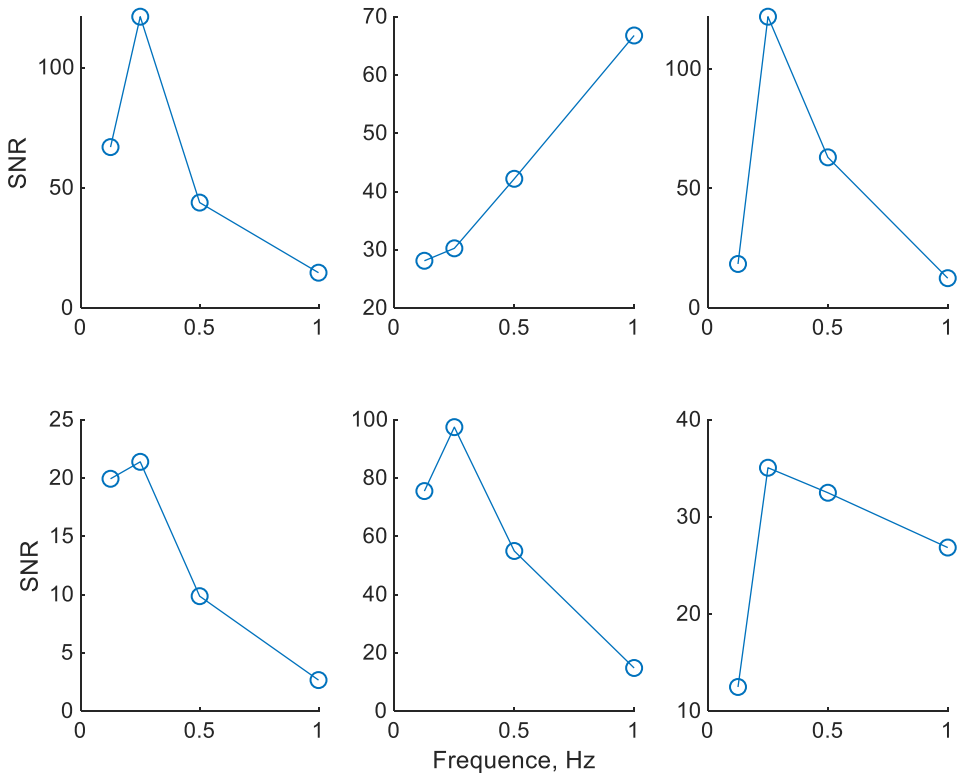

Figure 4 Frequency dependence of the signal-to-noise ratio (SNR). Each plot shows the SNR for a single observer for different mask periods (see details in the Methods).

The phase-locking analysis shows that the effectiveness of the mask is 20-30%. For slow speeds, the disappearance events are concentrated around a specific cycle phase. Additionally, the system spends a characteristic time in the invisible state. By jointly considering these three observations, we can conclude that a bar passing in the vicinity of the target induces a target to disappear, but not always. When the rotation speed is fast, so

that consecutive bars cross the target within a single disappearance epoch, a new disappearance event will not take place. Therefore, we would expect the statistics of the inter-disappearance events (the time between two consecutive disappearances) to correspond to the statistics of spontaneous disappearances under the limit of high rotation speed. If the rotation speed is too slow, there will be longer periods of visibility (resting states) between the induced invisible events, allowing for infrequent spontaneous events of disappearance (as in the Troxler effect) when the mask is in a favorable phase. In both cases, the distribution of the inter-disappearance times would be smeared across many timescales and would weakly depend on the stimulation frequency. For intermediate rotation speeds, where the rotation period is near the characteristic timescale of the system, upon a state switch triggered by a favorable stimulus event, the intrinsic dynamics bring the system to a resting state, thus to a response that is time locked to a specific phase and frequency. Since the mask does not induce a disappearance in every period, one would expect the inter-disappearance times to be predominantly multiples of the rotation period.

Figure 5 (top row) shows the inter-disappearance times for one observer. One can see that for mask periods (T) of 2, 4, and 8 seconds, there are peaks of the distributions of the inter-disappearance times corresponding to times nT, where n is an integer number, i.e., it frequently requires several mask periods before the target disappears. One can also observe that close to the stochastic resonance frequency (T = 4sec, Figure 5), the second and third times the bar passes the target (peaks at 8 and 12 sec) are more successful in inducing disappearance than the first time is. This is expected if the rotation period is slightly faster than the characteristic timescale of the system. Here, when the system returns to a resting state, the mask has already passed the most favorable phase for switching.

Another way to see the periodicity of the function is to take its Fourier transform. A single peaked amplitude spectrum will indicate a single dominant frequency. Computing the transform for sampled distributions is difficult, since there is no explicit form of the probability density function. However, the characteristic function (Billingsley, 1995) of the distribution is practically the Fourier transform of its probability density function (pdf). Since the pdf shape is not known, one may compute an empirical characteristic function (Cramér, 1946), and if the pdf is dominated by a periodic component, then a peak in the absolute value of the empirical characteristic function is expected. The middle row in Figure 5 shows the absolute value of the empirical characteristic function for samples whose histograms are shown in the top row. The peaks at the stimulation frequencies are clearly seen for mask periods of 2, 4, and 8 seconds (red circles) – confirming that the disappearance events are predominantly spaced by the integer number of periods (nT), with many different values for the integer n. Interestingly, the amplitude of the mode corresponding to stimulation frequency has a non-monotonic behavior)

(Figure 5, bottom row for all observers). For example, for the observer shown in the top and middle rows, the peak amplitude for T= 4 sec is larger than for T= 2 sec or T=8 sec.

Distributions and empirical characteristic functions for all observers are presented in the supplementary materials. The data for one observer (examples of raster plots are shown in Figure 2C,D) show no peak in the characteristic functions for any stimulation frequency. These results indicate the domination of noise in the behavior but may also reflect the low efficiency of bars as inducers for this observer. One of the indications for the first case is the similarity of the inter-disappearance distributions between moving bars, static bars, and Troxler conditions (Supplementary Figures Figure S2 1-6).

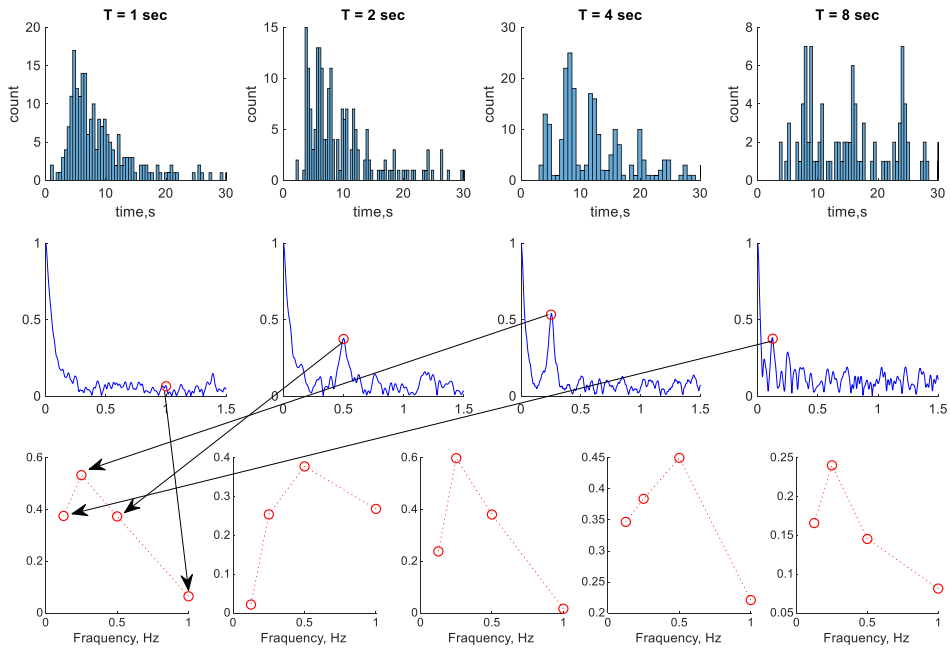

Figure 5. Inter-disappearance times. Top row: histograms of the inter-disappearance times for one observer during different mask periods (indicated in the subplot titles). Middle row: empirical characteristic functions of the distributions shown in the top row. Bottom row: Amplitudes from each characteristic function at the frequency corresponding to the frequency of the mask are shown. Each plot corresponds to the experiments performed by a single observer, with the left one matching the data depicted in the top and middle rows.

Discussion:

The series of experiments performed in this work indicate that rotating bars are effective inducers of target disappearance in MIB. Moreover, the effect is phase locked to the mask for long periods (Figure 2). We observed a refractory period for most observers (Figure 3). For the few other observers, there were many target disappearances in conditions with a static mask or without a mask (Troxler effect), suggesting either a low mask efficiency or a high intrinsic noise. Signal-to-noise analysis of the temporal sequences of responses showed stochastic resonance at frequencies around 0.25Hz, corresponding to a mask period of 4sec (Figure 4). Analyzing the empirical characteristic functions, we observed peaks at frequencies corresponding to integer multiples of mask periods (Figure 5). In other words, several mask periods are frequently required to induce a disappearance, indicating that moving bars are weak disappearance inducers and that the amount of intrinsic noise is relatively small. Additionally, in all experiments the distribution of invisibility times is well modeled by the sum of two random variables distributed according to gamma and the normal distributions. The Gamma distribution was frequently considered for describing switching dynamics in bistable systems. We added the Gaussian distribution to absorb temporal jitter when executing a motor command to press or release a keyboard key and the mean time required for a long excursion of the system until it returns to a resting state. In many different experiments the mean time in a Gaussian distribution predominantly varied between 1 and 2 seconds, with extreme values ranging from 0.5 sec to 2.5 sec. All of these properties are typical attributes of excitable systems in the presence of noise. Therefore, we concluded that the mechanisms responsible for MIB can operate in the regime of an excitable system.

One of the models used in the past to study bistable perception describes perceptual switches by the random motion of a “particle” in a double-well potential. In this model, the decision variable corresponds to a one-dimensional coordinate of a “particle” inside a potential with two local minima (two wells), separated by a barrier. In the absence of noise, the “particle” “falls down” to the position of the nearest local minimum and stays there forever. In the presence of noise, however, the “particle” has a chance to gain enough energy to overcome the barrier and move to another well and it will subsequently fall to another local minimum. Translating this to perception, it is usually assumed that when a “particle” is close to one minimum, one image is perceived, and when the “particle” is close to another minimum, another image is perceived. This one-dimensional model was introduced to study binocular rivalry by Kim et al., 2006. Nevertheless, it is hard to extend this formalism to describe the quasi-stable perception in MIB or the Troxler effect (Troxler, 1804). Here we suggest that the theory of excitable systems is a suitable framework for describing MIB. Although the practical implementation in a biological network can be quite complicated, the simplest formal model describing

excitable systems is the Fitzhugh-Nagumo model (FitzHugh, 1961; Nagumo et al., 1962; Sherwood, 2014). It assumes that the neuronal dynamics can be effectively described by two one-dimensional variables with substantially different timescales of evolution. The variable having fast dynamics can be interpreted as a decision variable in the double-well model. The variable with slow dynamics is assumed to represent processes such as adaptation (Caetta et al., 2007; Gorea & Caetta, 2009), filling-in (Hsu et al., 2006), motion streaks (Wallis & Arnold, 2009), depth ordering, and surface completion (Graf et al., 2002). Within this proposal, there is a perceptual criterion on the "fast" decision variable, so that a target is reported invisible when this criterion is crossed but is reported visible when the criterion crossing yielding a decision is in the opposite direction.

By changing parameters in the same noisy Fitzhugh-Nagumo model, one can describe other bistable phenomena such as binocular rivalry. This description can be general enough to describe all stable, bistable and quasi-stable perceptual phenomena. Furthermore, stable fixed points of the dynamical systems, forming attractors, constitute the basis for the memory models in the attractor neural networks (ANN). In these networks, the memory items are assumed to be recalled, or perceived, when the pattern of network activity is close enough to one of the stored patterns of activity (memory). Technically, when the overlap (correlation) between the activity and the stored memory exceeds some threshold value, the model is assumed to recall this stored memory. In other words, the overlap measure can be considered a decision variable. A memory item is then recalled (perceived as this specific item) when the dynamics of the network activity are near the memorized pattern (the fixed point of the dynamics), for example, the resting state in MIB or stable percepts in bistable phenomena. Thus, a possible interpretation of MIB follows, so that both the static target and the moving mask are separately consistent with some attractor states in the brain corresponding to their generated percepts, whereas both of them together are inconsistent with any attractor. Here, the mask plays the role of a force driving the network state away from an otherwise stable attractor that corresponds to the static target perception. It appears that there are no other stable attractors near the target (meaning that there is no stable illusory percept), and that the network dynamics relax (after a long excursion) into the stable state, yielding a visible target. During state transition, there is no stored pattern along the path of the dynamic that can be interpreted as target presence; therefore, the target stays perceptually invisible.

By considering the dynamics of the nonlinear systems near the bifurcation point in the context of the Attractor Neural Network model of memory, we speculate that the conscious state consists of activating a specific attractor associated with a specific memory. Once the network is driven away from the attractor, the brain becomes unaware of the physical stimulus until the network dynamics return to the memory attractor associated with any stimulus. Despite the brain being unaware of the physical stimulus,

the stimulus drives the dynamics of the network, allowing an interaction across the boundary of awareness (Meital-Kfir et al., 2016; Meital-Kfir & Sagi, 2018). As in the initial stage of testing these speculations, we established here that MIB could be considered as an excitable system.

Acknowledgment:

This work was supported by the Basic Research Foundation administered by the Israel Academy of Sciences and Humanities (grant No. 6501560).

Methods

Human Observers

This study was approved by the Weizmann Institute of Science Ethics Committee and the Helsinki Committee. Ten human observers with normal or corrected-to-normal vision participated in the experiment. Before experimentation, all observers provided their informed consent under the approved Declaration of Helsinki.

Six observers with normal or corrected-to-normal vision participated in all experiments.

Stimuli

This study included 6 experimental conditions. Stimuli consisted of a static target (yellow dot, 0.5 deg in diameter) placed at 6 deg in the upper-left visual field and a fixation point (white dot 0.25 deg in diameter). These elements were present in all conditions. In the Troxler condition, no additional elements were present on the screen. In the other (number) conditions, there was either a static or a rotating mask. The mask consisted of lines placed along six rays originating near the fixation point and form a 60° angle between each pair of rays. Each ray was composed of two distinguishable lines to avoid local interactions with the target during mask rotation. A similar "protection zone" was also kept between the mask and the fixation point. The inner line started at 1.25 deg of visual angle and ended at 4.6 deg, whereas the outer line started at 7 deg and ended at 10.5 deg. In the rotating mask conditions, the rays were rotated clockwise with constant angular velocity. The angular velocity was chosen so that the periods of motion (i.e., the time between identical images on the screen) were 1, 2, 4 or 8 sec.

Procedure

After signing a consent form, the observers performed several daily sessions (minimum 6, maximum-12). In each daily session, the observers performed three blocks of trials, 20 minutes each. A mandatory 15-minute break separated the blocks. Each trial was self-initiated by the observer and lasted 120 sec. During the trial, the observers were instructed to fixate on a central fixation point and report when the target is perceptually invisible by pressing and holding the space bar on a computer keyboard until the target becomes visible.

Empirical characteristic function

The characteristic function is formally defined as

$$\varphi_X(t) = E\left[e^{itX}\right]$$

where E[.] is the expected value, $i = \sqrt{-1}$ and X are random variables. Empirical distribution functions are computed by substituting samples from X

$$\varphi_X(t) = \sum_{k=1}^{n} e^{itx_k},$$

where x_k is the k -th data point out of n . Absolute values of $\varphi_X(t)$ are shown on graphs. $\varphi_X(0) = 1$ by definition, and if X has a periodic density function, there is only one non-zero value of $\varphi_X(t)$ corresponding to the period of density function.

Fitting procedure

We fitted the disappearance distributions as the sum of two random variables, one having a normal distribution and the other one having a Gamma distribution.

$$\begin{aligned} X &= X_1 + X_2 \\ X_1 &\sim \frac{1}{\sigma\sqrt{2\pi}} e^{-\frac{1}{2}\left(\frac{x-\mu}{\sigma}\right)^2} \\ X_2 &\sim \frac{1}{\Gamma(k)\theta^k} x^{k-1} e^{-\frac{x}{\theta}}, \end{aligned} \tag{1}$$

where $\Gamma(k)$ is a gamma function. The Gamma distribution was previously used to fit bistable phenomena (Carter & Pettigrew, 2003; Devyatko et al., 2017). Additionally, we assumed that there is a minimal delay required for the deterministic trajectory to return to a stable fixed point when the system is excited (the mean of the Normal distribution), and that some jitter exists in the motor responses, which we are attempting to capture by varying the variance of normal distribution. Although it is possible to compute the resulting distribution formally, estimations using the resulting formula are unstable; instead, we used many tuples of samples (10^5 for each set of parameters) where the first elements of a tuple consisted of samples from the normal distribution, and the second element of a tuple consisted of samples from the normal distribution. The values of tuples were added to have a sample from the theoretical distribution, which in turn, were used to form an empirical cumulative distribution, and finally, the intermediate values of the theoretical cumulative distribution function (CDF) were estimated by linear interpolation. Using interpolated CDF, we estimated the p-value of the Kolmogorov–Smirnoff goodness of fit. The obtained p-values were used as a cost function in an optimization procedure that consisted of 2 consecutive runs of Genetic Algorithm (GA (Deb, 1999), as implemented in Matlab ® optimization toolbox), followed by non-linear least-squares optimization. GA was scanned over different parameter values, and following a smooth

method, the local minimum near the best set of parameters was found by GA. Repeating this procedure with the best value found in the first round as seed values for a second round of GA increased the chances of finding better solutions. This method does not guarantee that no good fit to the data exists in cases where our procedure failed to find one.

Signal-to-Noise Ratio analysis

To compute the Signal-to-Noise Ratio (SNR), we created a signal representing the perceptual states as a function of time. The visible target was assigned the value '1' and the invisible target was assigned the value '0' discretized at 1ms precision. All trials were concatenated, sequentially forming a single signal for every observer. SNR was defined as the ratio between peak amplitude at a stimulation frequency within a narrow band (~2-10mHz) of an expected stimulation frequency and an average amplitude in a wider frequency window ($16\frac{2}{3}$ times wider). More specifically, a Fast Fourier Transform was computed on the generated signal and a narrow band was selected as 6 frequency bins around the expected frequency, whereas the wide band contained 100 frequency bins.

The details of exploratory experiment are provided in the Supplementary materials.

References

Billingsley, P. (1995). Probability and Measure - Third Edition. In *Wiley-Interscience Publication*.

Bonneh, Y. S., Cooperman, A., & Sagi, D. (2001). Motion-induced blindness in normal observers. *Nature*, *411*(6839), 798–801. https://doi.org/10.1038/35081073

Bonneh, Y. S., Donner, T. H., Cooperman, A., Heeger, D. J., & Sagi, D. (2014). Motion-Induced Blindness and Troxler Fading: Common and Different Mechanisms. *PLoS ONE*, *9*(3), e92894. https://doi.org/10.1371/journal.pone.0092894

Braun, J., & Mattia, M. (2010). Attractors and noise: Twin drivers of decisions and multistability. In *NeuroImage* (Vol. 52, Issue 3). https://doi.org/10.1016/j.neuroimage.2009.12.126

Caetta, F., Gorea, A., & Bonneh, Y. (2007). Sensory and decisional factors in motion-induced blindness. *Journal of Vision*, *7*(7). https://doi.org/10.1167/7.7.4

Cao, R., Pastukhov, A., Aleshin, S., Mattia, M., & Braun, J. (2021). Binocular rivalry reveals an out-of-equilibrium neural dynamics suited for decision-making. *ELife*, *10*. https://doi.org/10.7554/ELIFE.61581

Carter, O. L., & Pettigrew, J. D. (2003). A common oscillator for perceptual rivalries? *Perception*, *32*(3), 295–305. https://doi.org/10.1068/p3472

Cramér, H. (1946). Mathematical Methods of Statistics (PMS-9). In *Mathematical Methods of Statistics (PMS-9)*. https://doi.org/10.1515/9781400883868

Deb, K. (1999). Introduction to genetic algorithms. *Sadhana - Academy Proceedings in Engineering Sciences*, *24*(4). https://doi.org/10.1007/BF02823145

Devyatko, D., Appelbaum, L. G., & Mitroff, S. R. (2017). A Common Mechanism for Perceptual Reversals in Motion-Induced Blindness, the Troxler Effect, and Perceptual Filling-In. *Perception*, *46*(1), 50–77. https://doi.org/10.1177/0301006616672577

Duki, S. F., & Taye, M. A. (2018). Stochastic resonance and first arrival time for excitable systems. *Journal of Statistical Physics*, *171*(5). https://doi.org/10.1007/s10955-018-2031-z

FitzHugh, R. (1961). Impulses and Physiological States in Theoretical Models of Nerve Membrane. *Biophysical Journal*, *1*(6). https://doi.org/10.1016/S0006-3495(61)86902-6

Gammaitoni, L., Jung, P., & Marchesoni, F. (1998). *Stochastic resonance RMP p223_1.pdf*.

Gorea, A., & Caetta, F. (2009). Adaptation and prolonged inhibition as a main cause of motion-induced blindness. *Journal of Vision*, *9*(6), 16–16. https://doi.org/10.1167/9.6.16

Graf, E. W., Adams, W. J., & Lages, M. (2002). Modulating motion-induced blindness with depth ordering and surface completion. *Vision Research*, *42*(25). https://doi.org/10.1016/S0042-6989(02)00390-5

Hsu, L.-C., Yeh, S.-L., & Kramer, P. (2006). A common mechanism for perceptual filling-in and motion-induced blindness. *Vision Research*, *46*(12), 1973–1981. https://doi.org/10.1016/J.VISRES.2005.11.004

Jaworska, K., & Lages, M. (2014). Fluctuations of visual awareness: Combining motion-induced blindness with binocular rivalry. *Journal of Vision*, *14*(11), 11. https://doi.org/10.1167/14.11.11

Kim, Y.-J., Grabowecky, M., & Suzuki, S. (2006). Stochastic resonance in binocular rivalry. *Vision Research*, *46*(3), 392–406. https://doi.org/10.1016/J.VISRES.2005.08.009

Lindner, B., García-Ojalvo, J., Neiman, A., & Schimansky-Geier, L. (2004). Effects of noise in excitable systems. *Physics Reports*, *392*(6), 321–424. https://doi.org/10.1016/J.PHYSREP.2003.10.015

Longtin, A., & Chialvo, D. R. (1998). Stochastic and deterministic resonances for excitable systems. *Physical Review Letters*, *81*(18), 4012–4015. https://doi.org/10.1103/PhysRevLett.81.4012

Meital-Kfir, N., Bonneh, Y. S., & Sagi, D. (2016). Asymmetric visual interactions across the boundary of awareness. *Journal of Vision*, *16*(10), 4–4. https://doi.org/10.1167/16.10.4

Meital-Kfir, N., & Sagi, D. (2018). Real-time visual interactions across the boundary of awareness. *Scientific Reports*, *8*(1), 6442. https://doi.org/10.1038/s41598-018-24554-1

Muratov, C. B., Vanden-Eijnden, E., & E., W. (2005). Self-induced stochastic resonance in excitable systems. *Physica D: Nonlinear Phenomena*, *210*(3–4), 227–240. https://doi.org/10.1016/J.PHYSD.2005.07.014

Nagumo, J., Arimoto, S., & Yoshizawa, S. (1962). An Active Pulse Transmission Line Simulating Nerve Axon*. *Proceedings of the IRE*, *50*(10). https://doi.org/10.1109/JRPROC.1962.288235

Sherwood, W. E. (2014). FitzHugh–Nagumo Model. In *Encyclopedia of Computational Neuroscience* (pp. 1–11). https://doi.org/10.1007/978-1-4614-7320-6_147-1

Sparrow, J. E., LaBarre, J. A., & Merrill, B. S. (2017). Individual differences in motion-induced blindness: The effects of mask coherence and depth ordering. *Vision Research*, *141*, 117–126. https://doi.org/10.1016/J.VISRES.2016.11.008

Troxler, I. P. v. (1804). Uber das Verschwinden gegebener Gegenstande innerhalb unseres Gesichtskreises. *Ophthalmologische Bibliothek*, *2*(2).

Versteegen, R., Gimel'farb, G., & Riddle, P. (2016). Texture modelling with nested high-order Markov–Gibbs random fields. *Computer Vision and Image Understanding*, *143*, 120–134. https://doi.org/10.1016/J.CVIU.2015.11.003

Volkov, E. I., Ullner, E., Zaikin, A. A., & Kurths, J. (2003). Oscillatory amplification of stochastic resonance in excitable systems. *Physical Review E - Statistical Physics, Plasmas, Fluids, and Related Interdisciplinary Topics*, *68*(2), 7. https://doi.org/10.1103/PhysRevE.68.026214

Wallis, T. S. A., & Arnold, D. H. (2009). Motion-Induced Blindness and Motion Streak Suppression. *Current Biology*, *19*(4). https://doi.org/10.1016/j.cub.2008.12.053

Supplementary materials

Disappearance patterns for individual observers

Below are figures of the disappearance patterns for all 6 observers presented in the format of Figure 1. Each column represents one rotation period - 1, 2, 4, and 8 seconds from left to right.

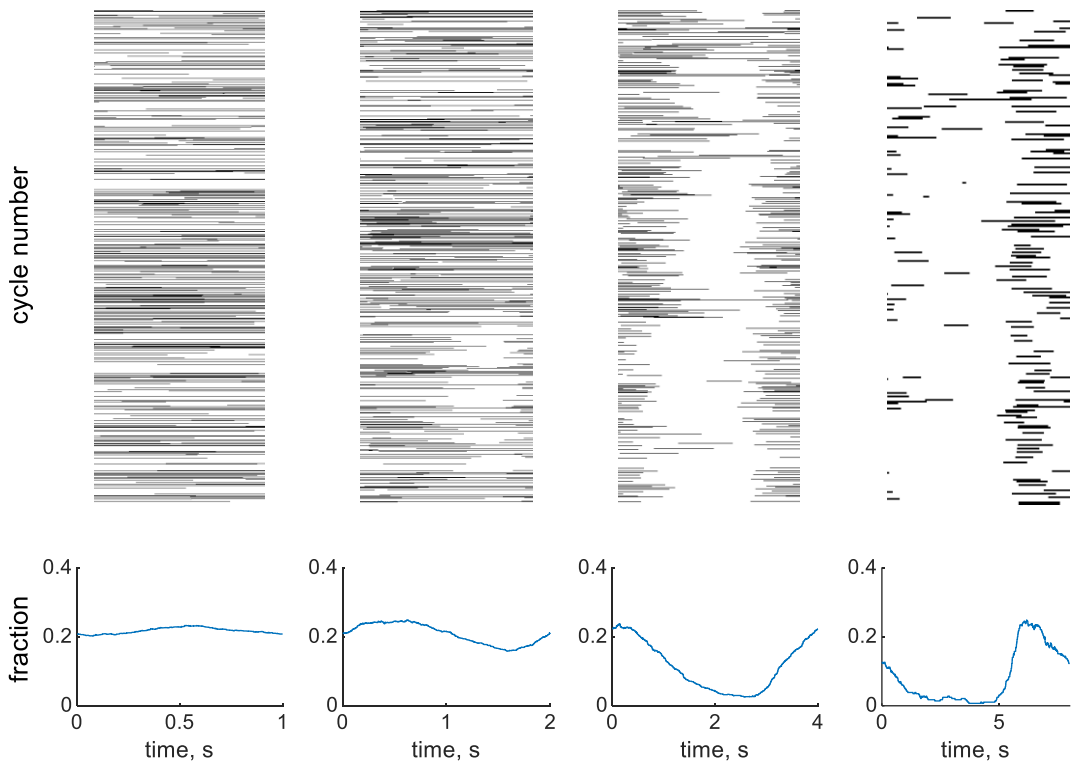

Figure S.1. 1 Disappearance patterns for observer O1.

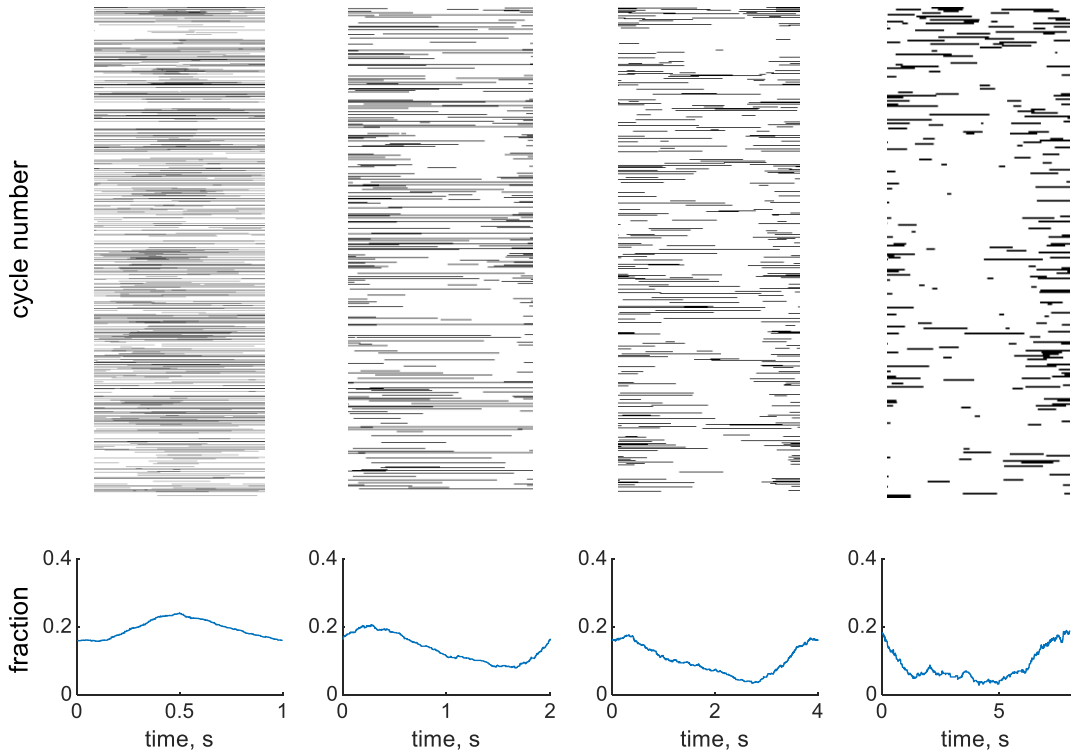

Figure S.1. 2 Disappearance patterns for observer O2.

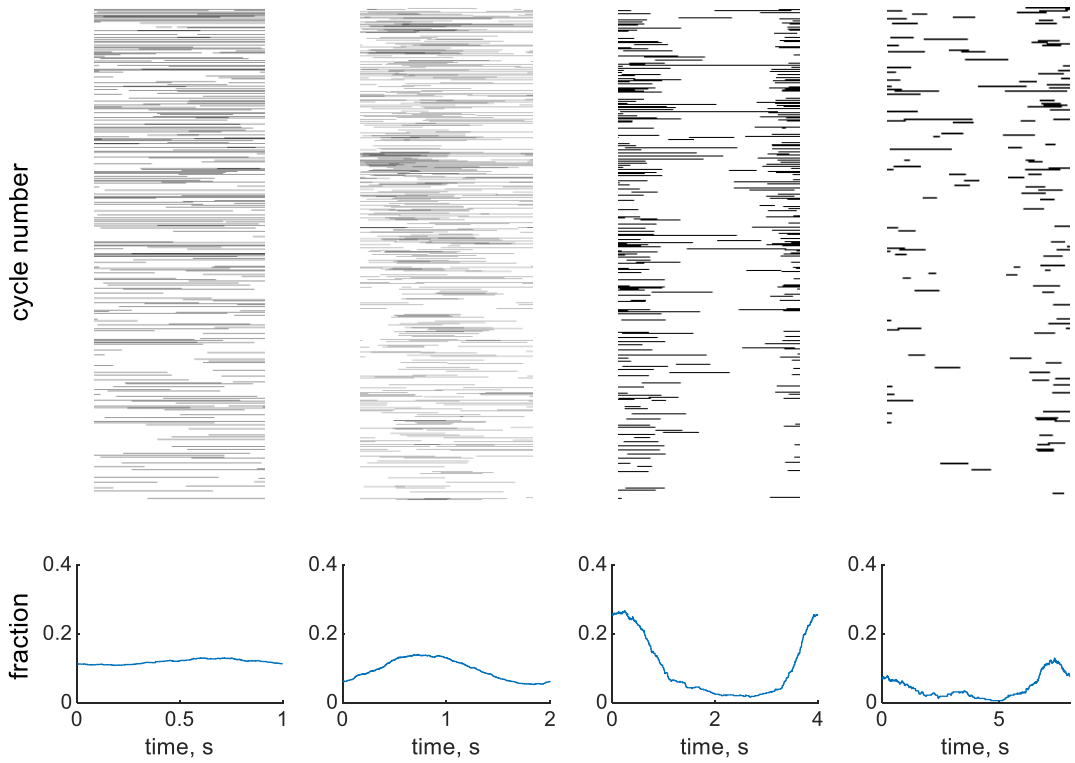

Figure S.1. 3 Disappearance patterns for observer O3.

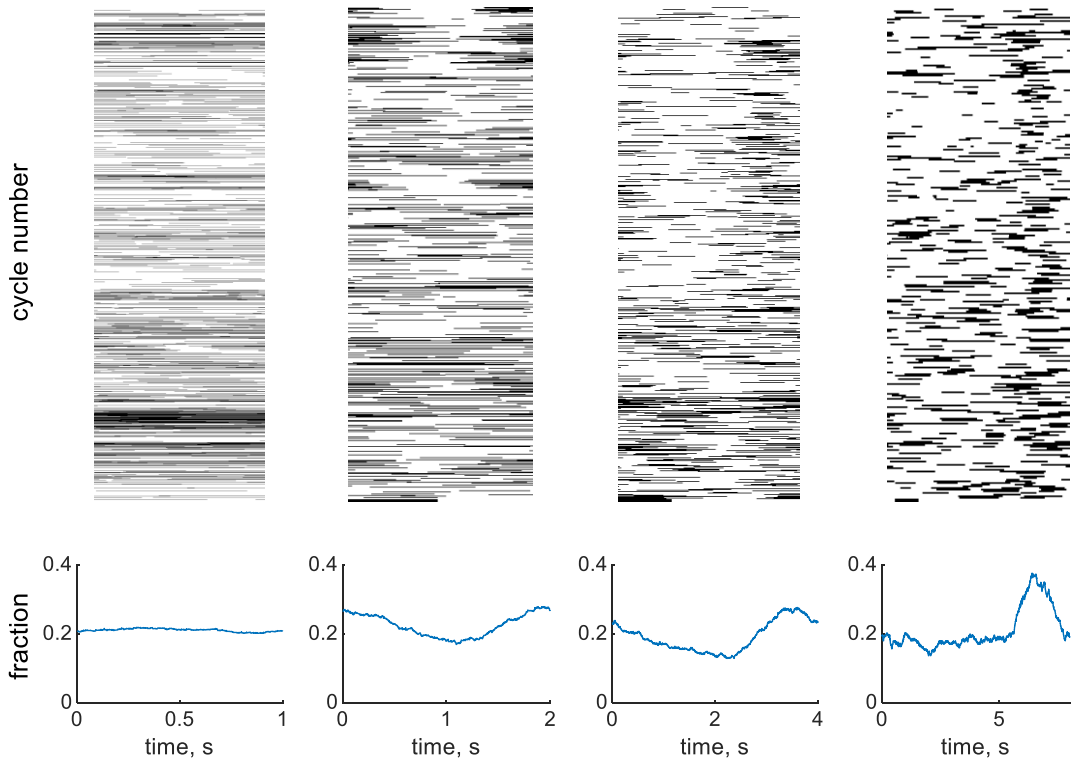

Figure S.1. 4 Disappearance patterns for observer O4.

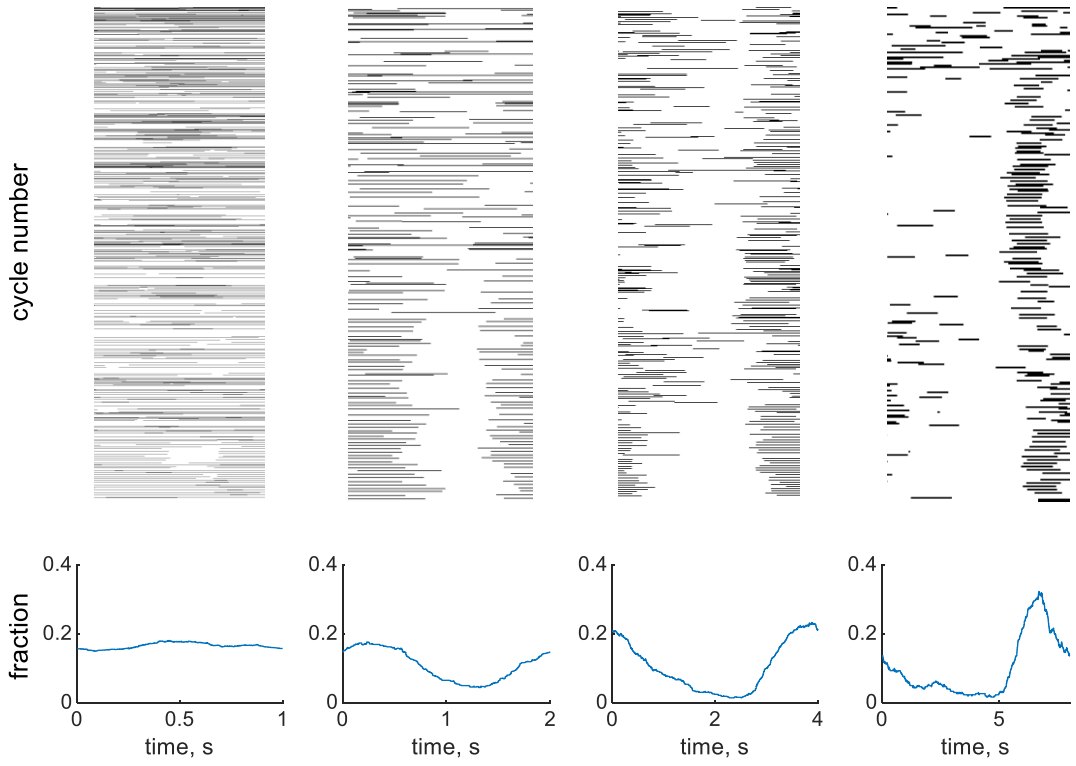

Figure S.1. 5 Disappearance patterns for observer O5.

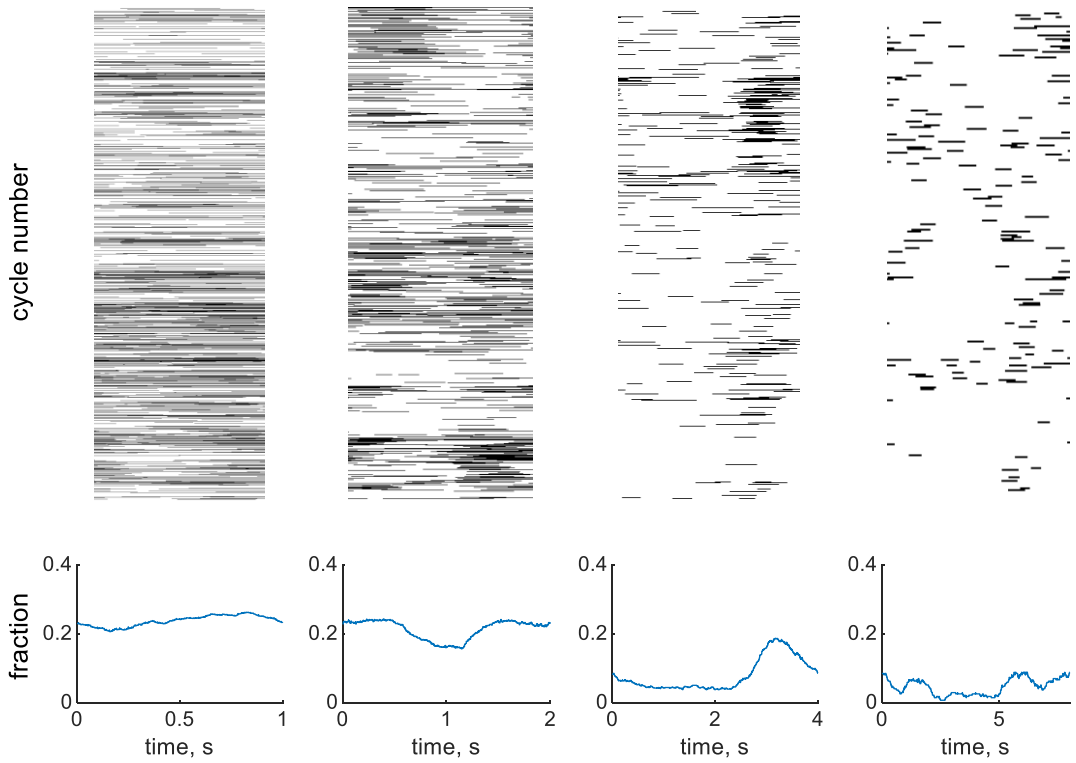

Figure S.1. 6 Disappearance patterns for observer O6.

Inter-disappearance times for all observers

Below are the inter-disappearance times for all 6 observers. Each figure shows the results obtained in different conditions (row) for one observer. The left column shows the distribution of the inter-disappearance times, the right column, the empirical characteristic function. The characteristic function for strictly periodic distributions would have a peak at the frequency corresponding to a period. The conditions are (from bottom to top) Troxler, a static mask, and a rotating mask with periods of 1, 2, 4, and 8 seconds. The distributions are not shown if there were fewer than 5 disappearance events.

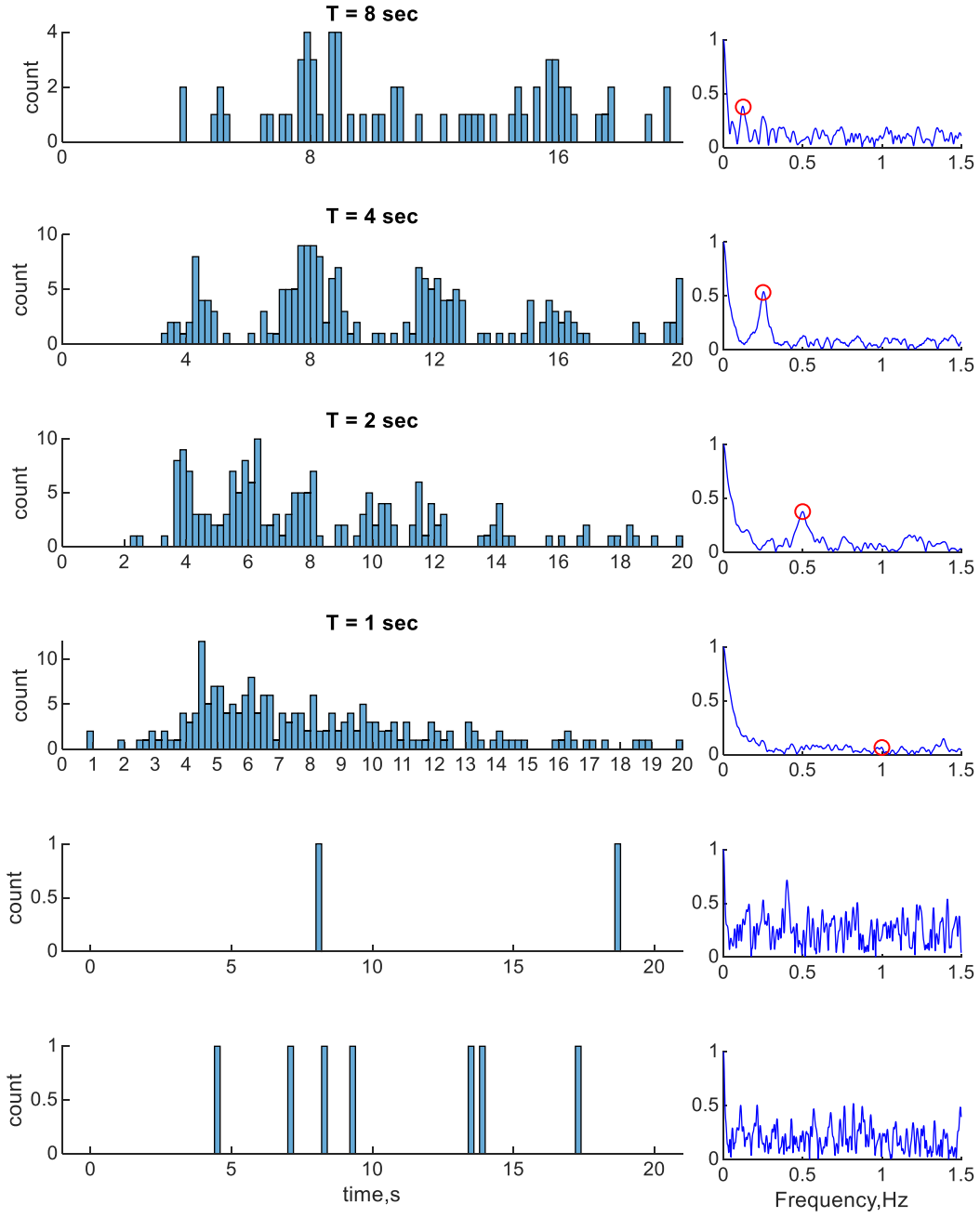

Figure S2 1 Inter-disappearance times for observer O1. The bottom row shows the results for the static mask condition, and one row above it shows the results for the Troxler effect (no mask present).

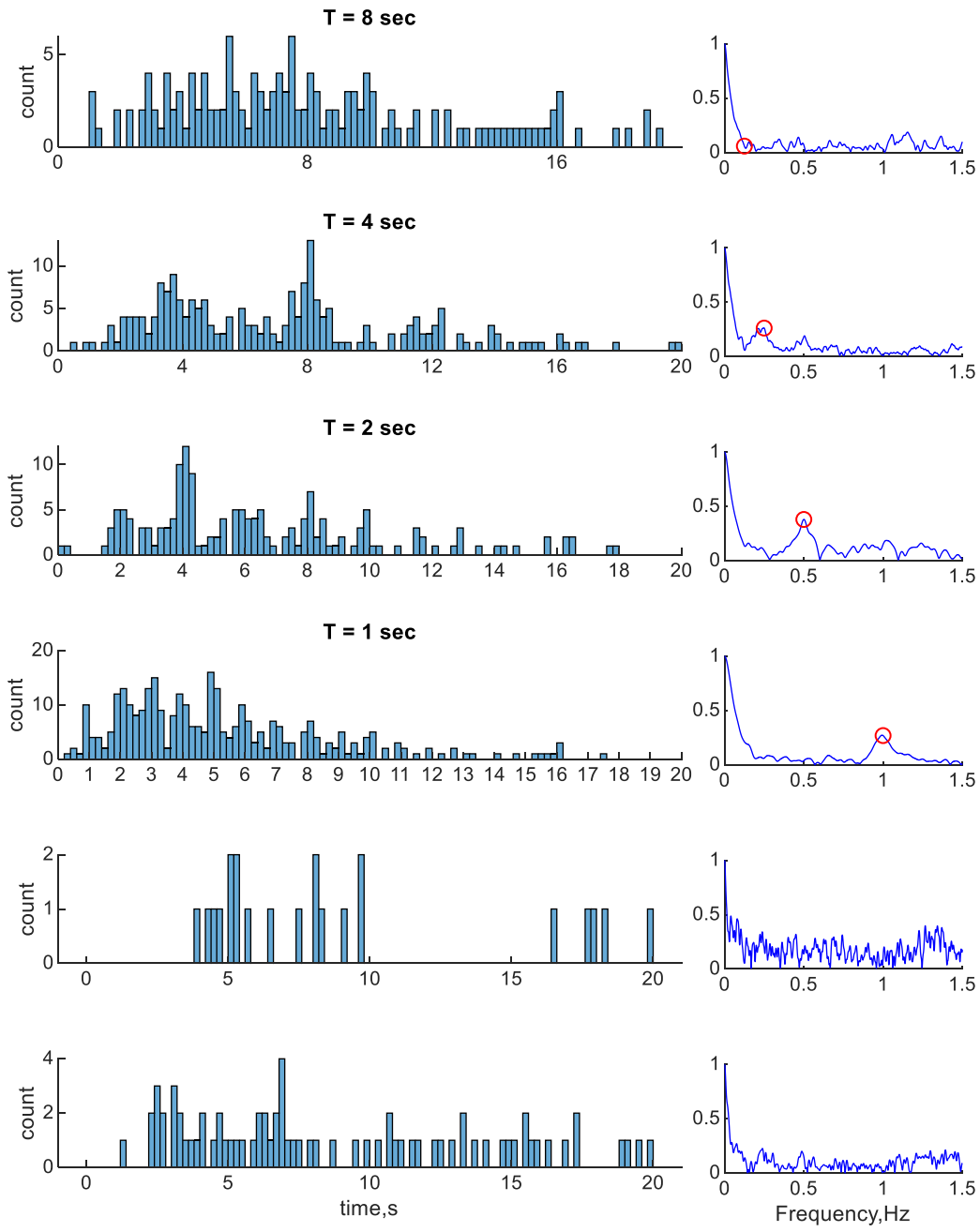

Figure S2 2 Inter-disappearance times for observer O2

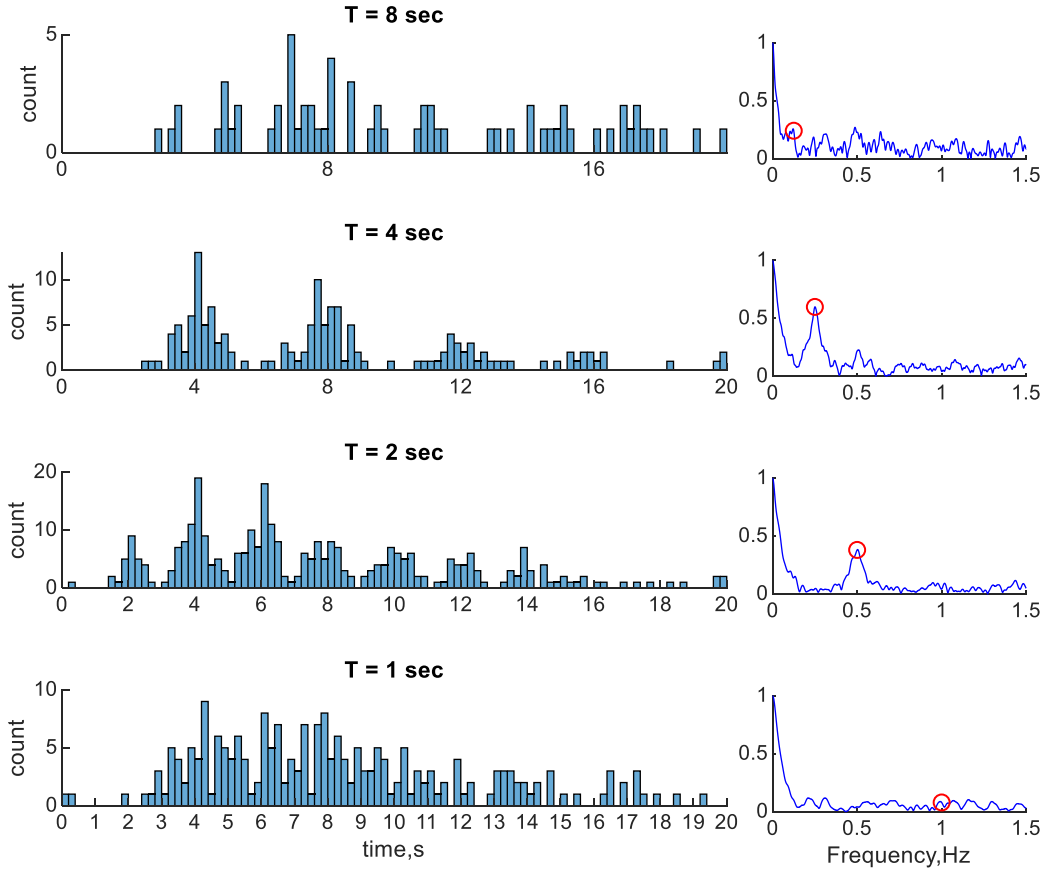

Figure S2 3 Inter-disappearance times for observer O3

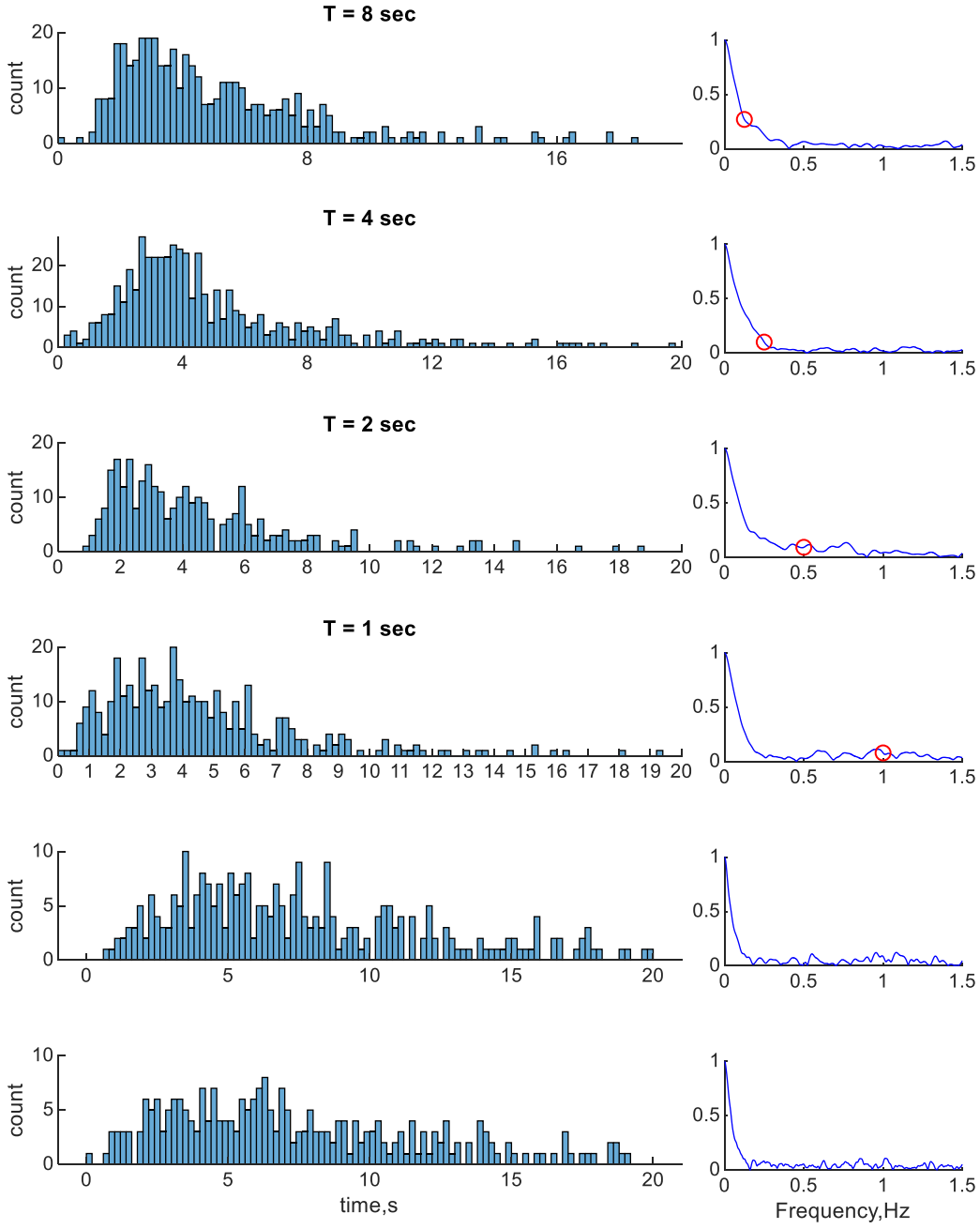

Figure S2 4 Inter-disappearance times for observer O4

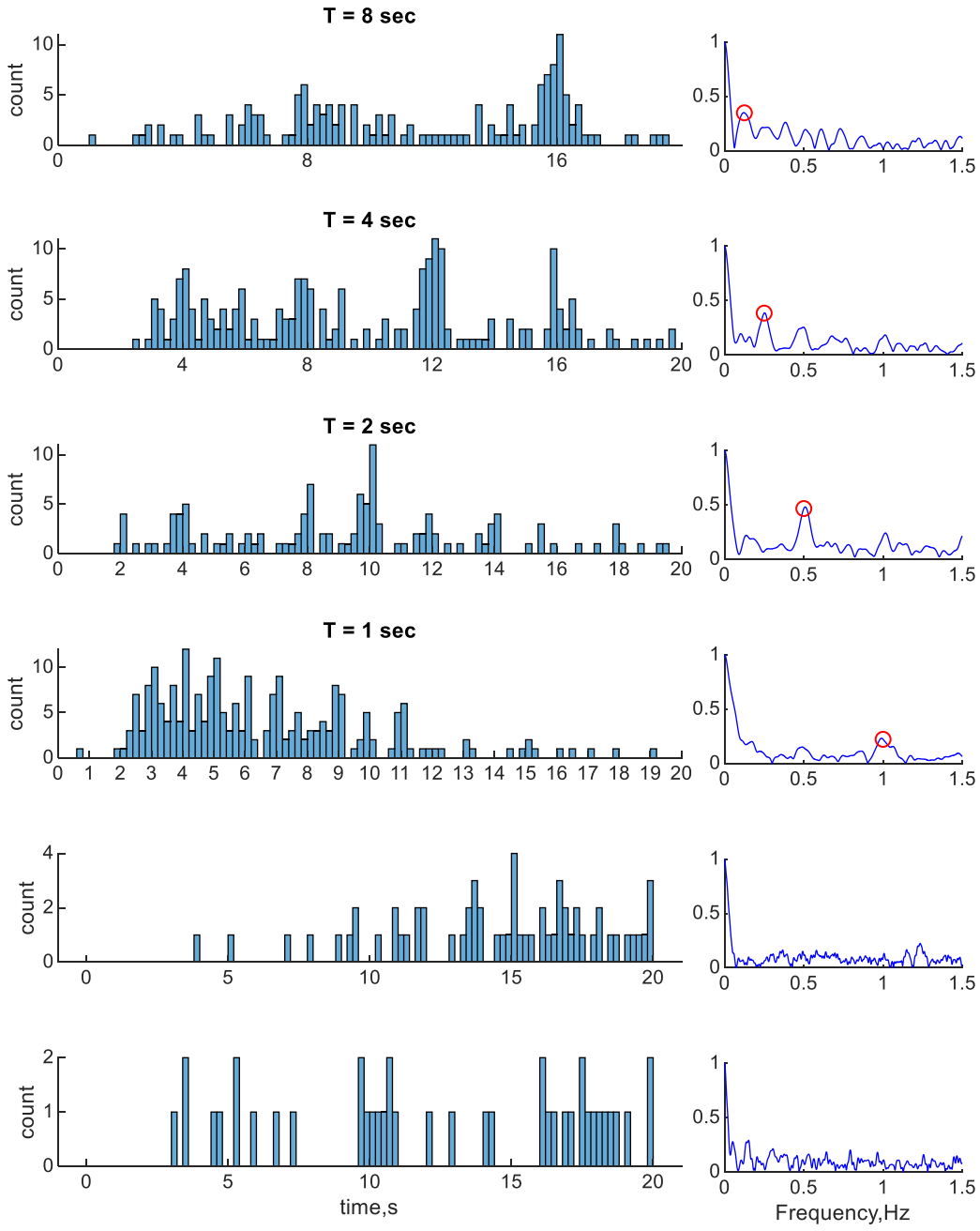

Figure S2 5 Inter-disappearance times for observer O5

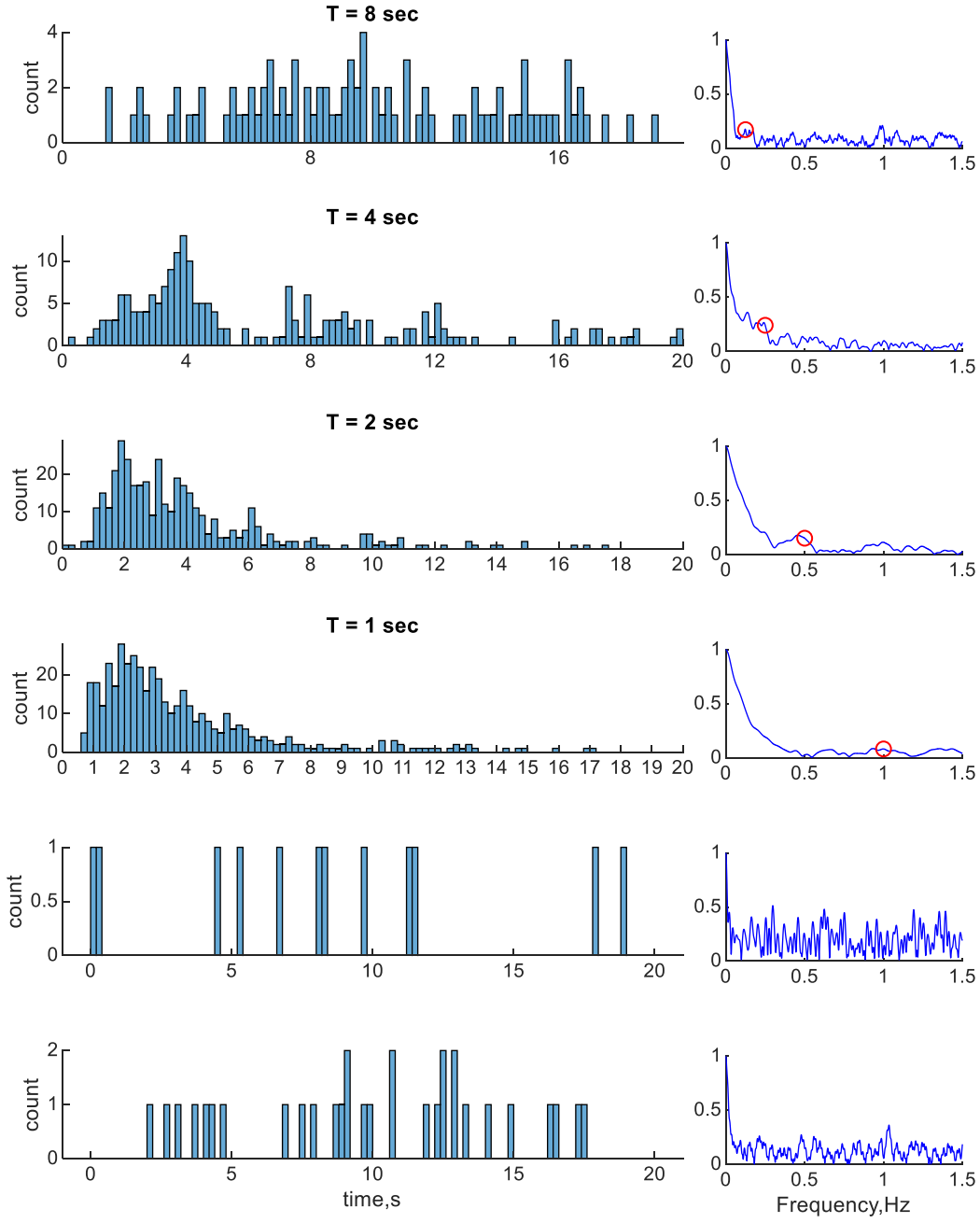

Figure S2 6 Inter-disappearance times for observer O6

Distributions of visible and invisible periods for all observers

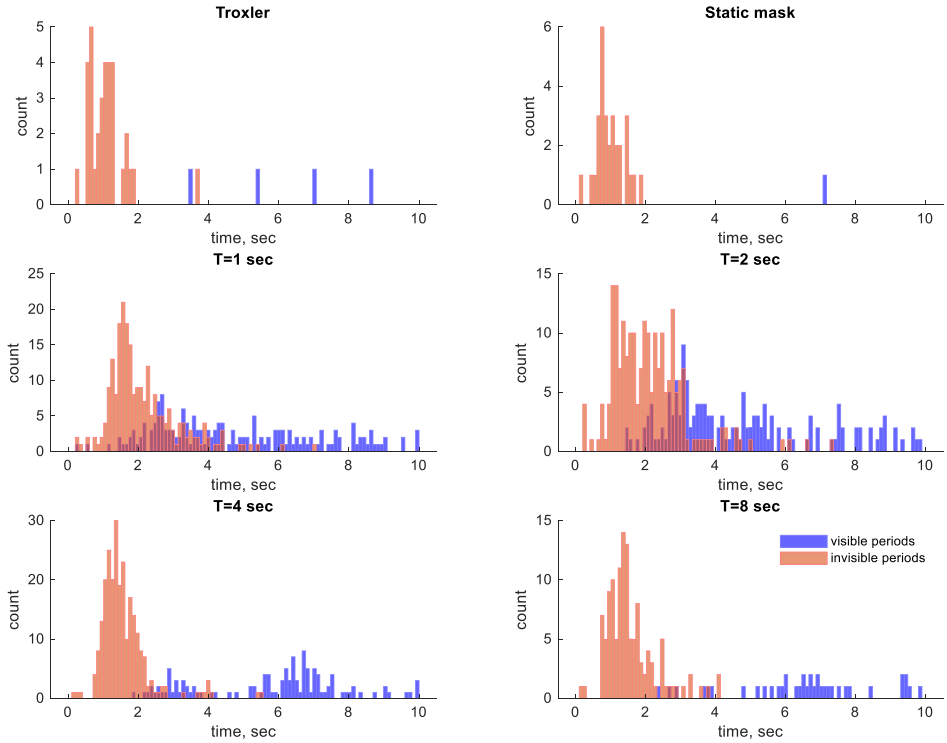

Figure S3 1 Distributions of the visible and invisible periods for observer O1

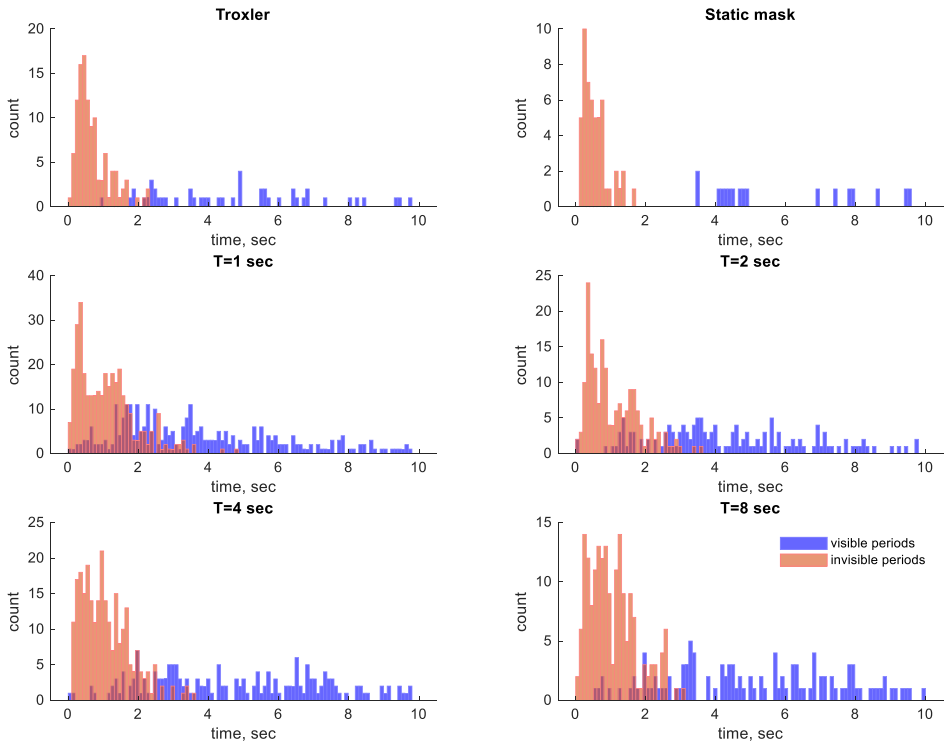

Figure S3 2 Distributions of the visible and invisible periods for observer O2

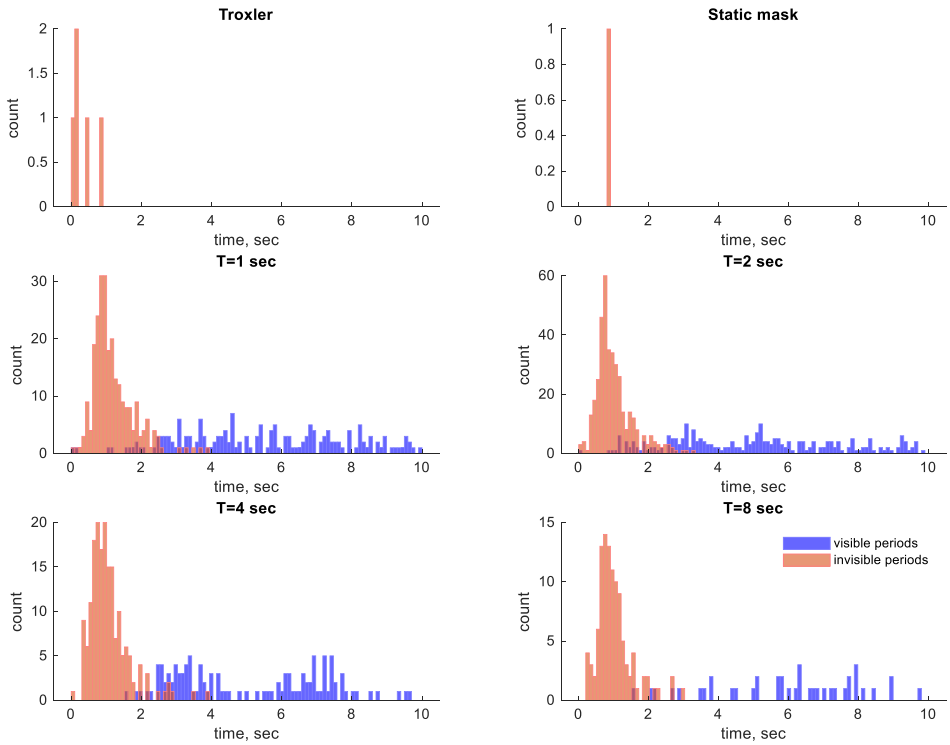

Figure S3 3 Distributions of the visible and invisible periods for observer O3

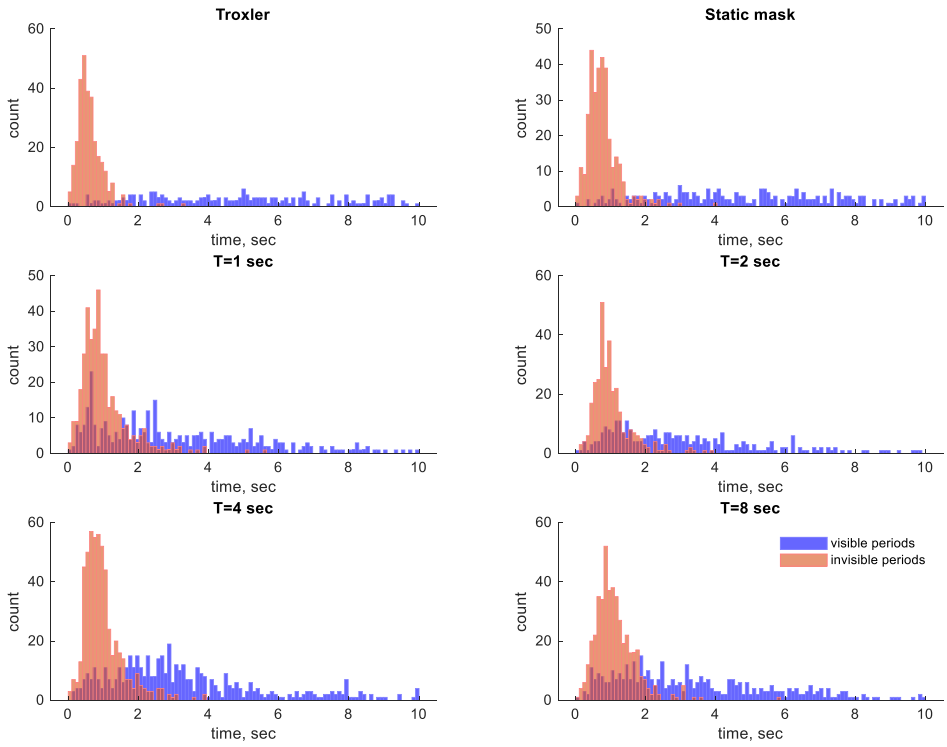

Figure S3 4 Distributions of the visible and invisible periods for observer O4

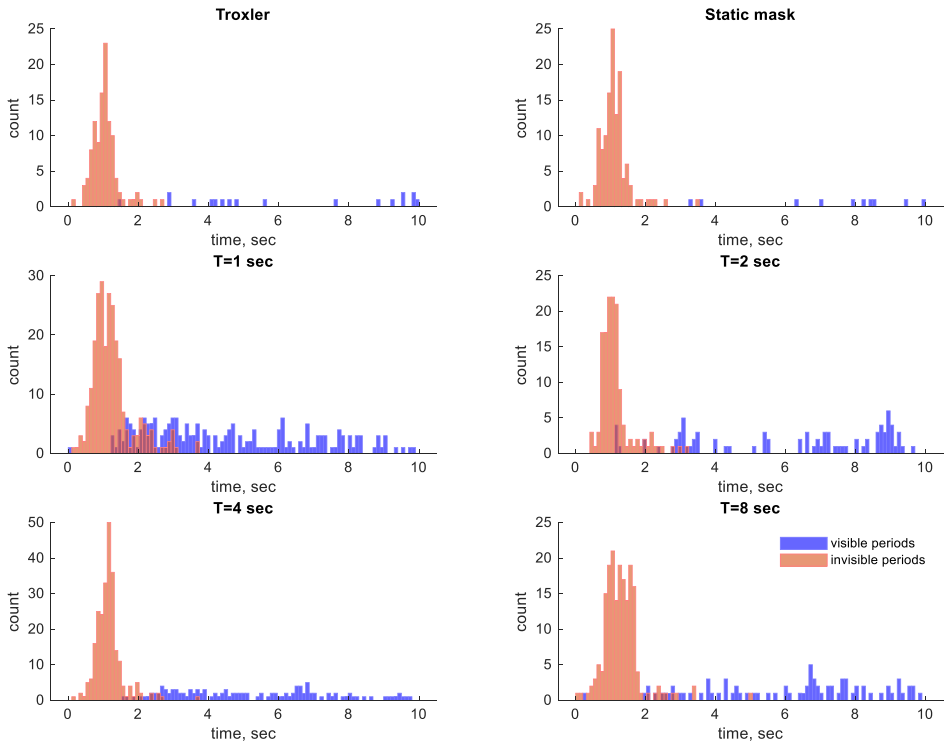

Figure S3 5 Distributions of the visible and invisible periods for observer O5

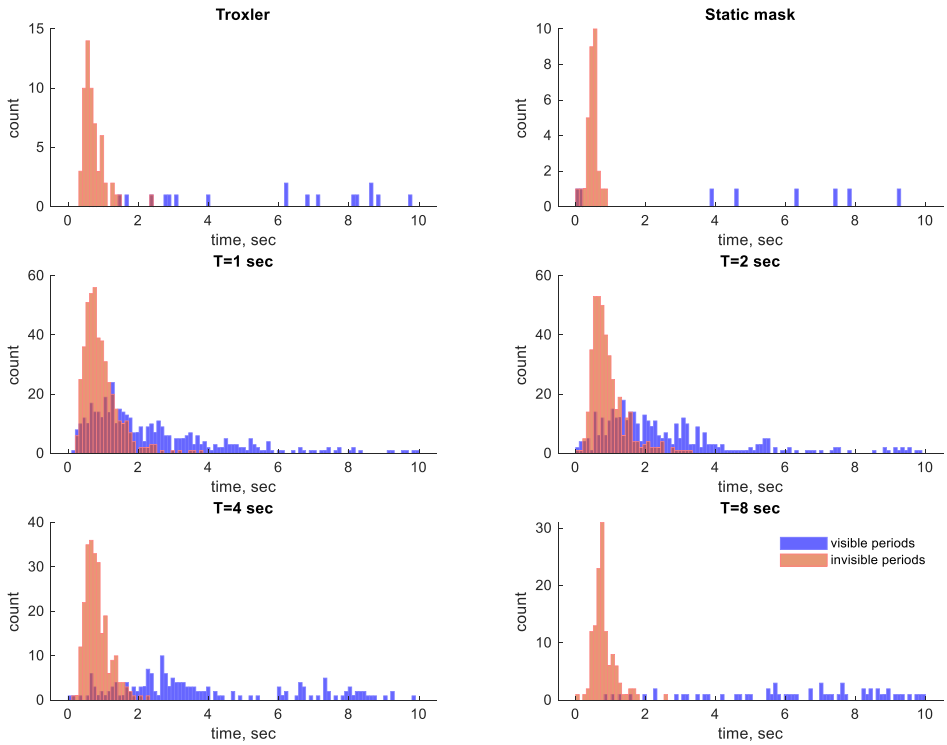

Figure S3 6 Distributions of the visible and invisible periods for observer O6

The distribution parameters in the exploratory experiments

There were many experiments in different conditions. In the table below we show the parameters of the fit for the sum of the normal and Gamma distributions. Only 7 p-values (out of 112) are below 0.05.

κ	θ	μ	σ	p
0.67	0.9	0.41	0.1	0.89
0.68	0.31	0.15	0.03	0
0.77	0.42	0.46	0.22	0.38
0.81	0.35	0.48	0.2	0.18
0.44	0.67	0.68	0.34	0.35
0.82	0.1	0.9	0.34	0.71
0.09	1.38	0.99	0.31	0.54
0.82	1.58	1.42	0.58	0.91
0.39	0.55	1.17	0.43	0.79

0.87	2	0.38	0.04	0
0.59	0.27	1.25	0.55	0.86
0.51	0.36	1.06	0.44	0.79
1.1	1.39	0.24	0.03	0.65
1.59	0.88	0.53	0.35	0.97
1.68	0.67	0.49	0.3	0.86
0.43	0.63	1.13	0.52	0.96
0.3	0.59	1.16	0.19	0.79
0.31	0.36	1.35	0.23	0.97
1.12	0.28	0.95	0.15	0.62
0.21	0.52	1.24	0.28	0.92
2.37	0.18	0.87	0.08	0.98
0.54	0.03	1.17	0.32	0.02
0.5	0.24	0.89	0.15	0.28
0.16	0.42	1.2	0.25	0.24
0.96	0.01	1.02	0.16	0.3
0.53	0.39	1.09	0.27	0.88
0.4	0.46	1.32	0.33	0.85
0.21	0.19	1.25	0.35	0.58
0.71	0.2	1.02	0.31	0.53
0.26	0.07	1.27	0.29	0.19
0.38	0.39	1.11	0.17	0.62
0.3	0.02	1.23	0.28	0.04
0.26	0.45	1.39	0.29	0.68
0.24	0.22	1.33	0.34	0.7
0.1	0.32	1.23	0.27	0.52
0.15	0.27	1.07	0.2	0.56
0.69	0.15	1.31	0.27	0.6
0.84	0.17	1.27	0.2	0.77
0.07	0.41	1.47	0.22	0.46
0.54	0.1	1.31	0.24	0.62
1.63	0.08	1.02	0.21	0.9
0.53	0.13	1.53	0.37	0.83
0.49	0.13	1.57	0.47	0.52
0.22	0.21	1.37	0.32	0.7
0.18	0.58	1.09	0.18	0.3
0.2	0.28	1.28	0.22	0.4
0.2	0.48	1.2	0.2	0.28
0.35	0.1	1.2	0.25	0.32
0.94	0.21	1.11	0.15	0.17

1.68	0.08	1.11	0.21	0.04
0.3	0.25	1.29	0.2	0.52
0.8	0.13	1.13	0.21	0.6
0.55	0.45	1.08	0.17	0.33
0.56	0.13	1.19	0.23	0.39
0.36	0.45	1.06	0.21	0.38
0.81	0.28	1.48	0.3	0.74
0.39	0.63	1.45	0.34	0.63
0.29	0.59	1.23	0.16	0.72
0.19	0.49	1.26	0.26	0.67
0.05	0.34	1.46	0.24	0.3
0.25	0.61	1.17	0.22	0.54
1.84	0.18	0.97	0.19	0.56
0.38	0.27	1.21	0.17	0.91
0.55	0.11	1.53	0.29	0.83
0.48	0.14	1.35	0.22	0.61
2.03	0.08	1.24	0.24	0.6
1.41	0.08	1.29	0.29	0.35
1.2	0.07	1.23	0.22	0.63
0.23	0.34	1.26	0.24	0.82
0.66	0.34	1.08	0.19	0.47
0.15	0.33	1.4	0.7	0.59
0.3	0.63	1.54	0.64	0.68
0.33	0.48	1.62	0.6	0.7
0.72	1.01	1.09	0.73	0.89
1.38	0.85	0.62	0.41	0.97
0.57	0.38	1.14	0.56	0.91
0.16	0.18	1.67	0.5	0.93
0.45	0.62	1.35	0.38	1
0.89	0.42	1.87	0.26	0.15
1.27	0.32	1.98	0.14	0.88
1.49	0.22	1.96	0.25	0.69
0.67	0.71	1.32	0.28	0.49
0.24	0.8	1.71	0.31	0.83
1.28	0.35	1.99	0.17	0.04
1.91	0.14	1.65	0.26	0.67
1.9	0.39	2.13	0.15	0.05
1.58	0.35	1.92	0.01	0
0.9	0.44	1.93	0.27	0.76
0.98	0.35	1.72	0.25	0.54

0.15	0.29	1.65	0.34	0.69
0.41	0.69	1.57	0.22	0.64
1.42	0.55	1.91	0.53	0.65
1.2	0.83	1.38	0.46	0.98
2.2	1.9	1.84	0.35	0.05
1.88	0.57	2.43	0.93	0.4
1.77	0.95	2.06	0.45	0.14
1.74	0.42	2	0.53	0.18
1.88	1.58	1.55	0.85	0.93
1.66	0.75	1.81	0.59	0.96
0.57	0.62	1.52	0.58	0.78
1.45	0.05	1.56	0.43	0.64
1.3	0.72	0.71	0.39	0.97
0.69	1.14	1.35	0.69	0.98
1.5	0.97	0.76	0.28	0.97
0.62	1.08	1.27	0.52	0.99
1.62	1.34	0.56	0.67	0.86
1.42	1.05	0.53	0.08	0.89
0.98	1.17	0.71	0.15	0.93
0.75	0.94	1.05	0.56	0.8
0.17	1.78	1.56	0.58	0.99
1.55	1.15	0.67	0.53	0.96
0.99	1.5	0.74	0.05	0.75

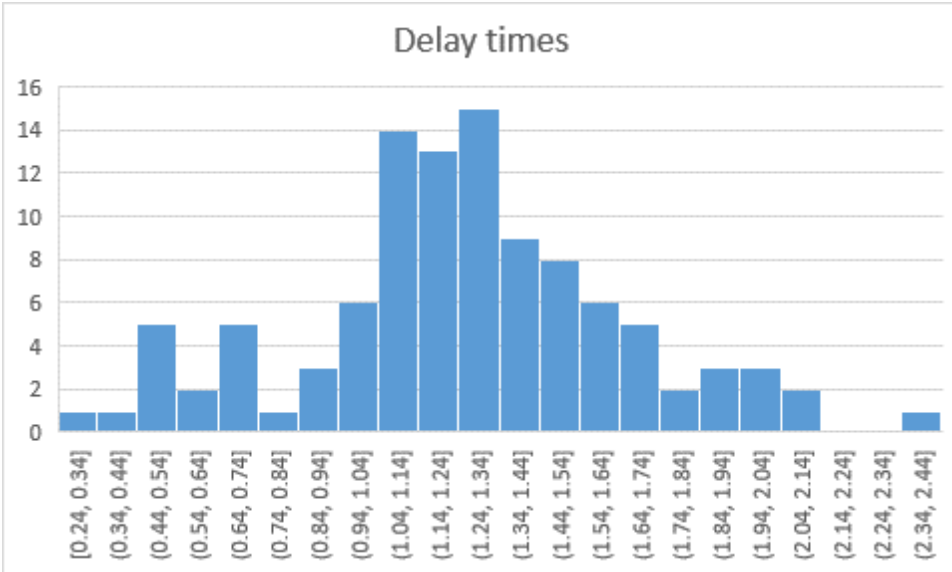

Figure S4. Distribution of the fixed delays. There is a minimal gap of .24 sec (excluding bad fits) and a typical value is of the order of one second. Presumably this is the time it takes for the system to return to a resting state once excited.

Fitzhugh-Nagumo. Basics

We assume that the stable perception is reflected in a stable fixed point in the dynamics of the two-dimensional decision model. We would also assume that both variables are noisy, reflecting background neuronal activity not related to the stimulus in question. The illustrative example of such a system is the FitzHugh–Nagumo class of models (FHN, (FitzHugh, 1961; Nagumo et al., 1962; Sherwood, 2014)), which can be described (without noise) by following a set of differential equations

$$\begin{aligned} \frac{\partial v}{\partial t} &= av(v-b)(c-v) - w + I_{ext} \\ \tau \frac{\partial w}{\partial t} &= v - dw + e, \end{aligned} \tag{1}$$

where v is a decision variable, w is a recovery variable, I_{ext} is an external input, τ is a relative time constant of a recovery variable, and a, b, c, d and e are some constants defining the behavior of a dynamical system. This dynamical system has a few prototypical behaviors that can be understood by analyzing its phase diagram.

The basic analysis of dynamical systems is performed by examining conditions when the right side of the differential equation is equal to zero. In this situation, the corresponding variable does not change at a particular moment. All the points where such a condition is satisfied for a single differential equation are called a nullcline. Since there are two equations in System (1), there are two nullclines (Figure S 1). The point where all (two in this case) nulclines intersect (if such a point exists) is a fixed point of a dynamical system, i.e., in the absence of noise, the dynamical system will stay at this point forever if the dynamics start at this point. Nevertheless, in the presence of noise, there are two types of system behavior: a stable fixed point - when any small perturbation of the system due to noise or due to a force will be counteracted by the dynamical system and the system returns to the fixed point or an unstable fixed point – when small perturbations are amplified by the dynamical system and the system will move away from the fixed point – this is referred to as an unstable fixed point. The FHN system may have 1, 2, or 3 fixed points, depending on the parameters.

One can see that the nullcline for the first differential equation is cubic, which in general has one local minimum and one local maximum (the blue curves in Figure S 1). For stability reasons, it is important that on the left side the curve goes to plus infinity, whereas on the right side it goes to minus infinity. The second nullcline is a straight line with positive slope (the orange line in Figure S 1). The behavior of the system depends on where the nullclines intersect. If a linear nullcline intersects a cubic nullcline on the left side of the local minimum (Figure S 1a), this intersection point will be a stable fixed point, i.e., the dynamical system will approach this point. In contrast, if a linear nullcline intersects a cubic nullcline in between the local minimum and maximum (Figure S 1b), the fixed point is unstable, and the system, even if it visits, (in the presence of noise) will move away from this point. This FHN regime leads to oscillatory behavior. The third interesting possibility is when a linear nullcline intersects a cubic nullcline before the minimum, between the minimum and maximum, and after the maximum (Figure S 1c). Here, the system has two stable fixed points. Therefore, in general we have the following cases: No stable fixed point (a linear nullcline intersects a cubic only between the local minimum and maximum) – the system undergoes oscillations. If there is one stable fixed point on the left side of the minimum or on the right side of the maximum (the system will end up near those points in the presence of small noise). If there are two stable fixed points on the left side of the local minimum and on the right side of the local maximum, the system will end up in one of the minima, depending on the initial conditions. In the presence of noise, FHN with parameters leading to 2 stable fixed points may be used to describe bistable phenomena, whereas FHN with parameters leading to a single fixed point may be used to describe the MIB.

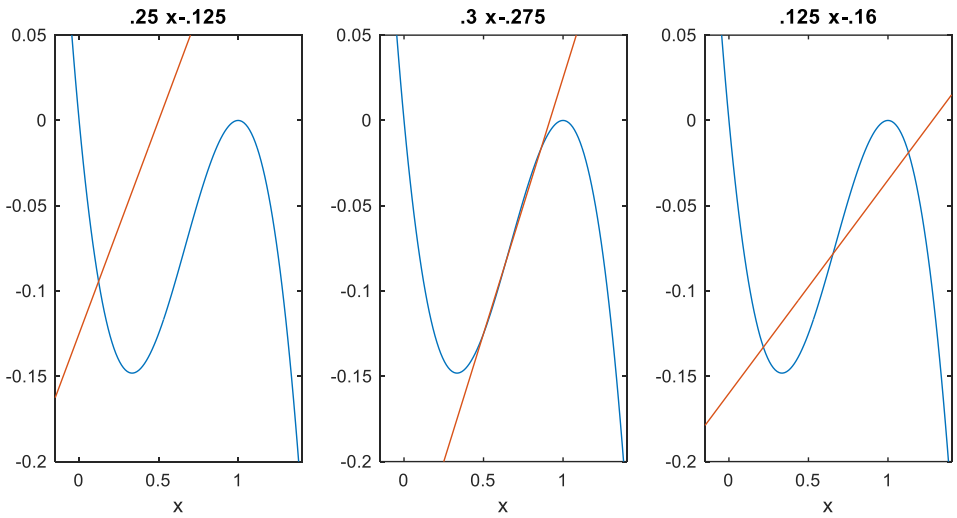

Figure S 1 Nullclines for 3 different regimes in the Fitzhugh-Nagumo model.

To describe MIB as an excitable system, one needs to make an additional assumption that a threshold exists on the fast variable V, so that when the system is on the right side of the threshold the target is perceived as invisible, and when the system is on the left side of the threshold the target is perceived as visible (see Figure S *2*). The mask can be considered to contribute to external input, which formally moves a cubic in a vertical direction, whereas the linear nullcline stays at the same place. When a cubic nullcline is driven up, the fixed point moves toward a bifurcation point (where the linear nullcline intersects the cubic in a local minimum), after which there is no stable fixed point. The interpretation would be that if there is a strong enough external input, the system will be excited by it and start a large trajectory. In the presence of noise, the closer the fixed point is to the bifurcation, the easier it is for the noise to excite the system. That is what probably happens when the mask bars approach a target – the fixed point is moved closer to the bifurcation point. Since invisibility is not induced every time the mask bar crosses the target, the fixed point does not cross the bifurcation point; moreover, the noise is relatively small in order to induce transition. However, since the invisibility periods are phase locked to the mask, the fixed point is probably moved substantially.

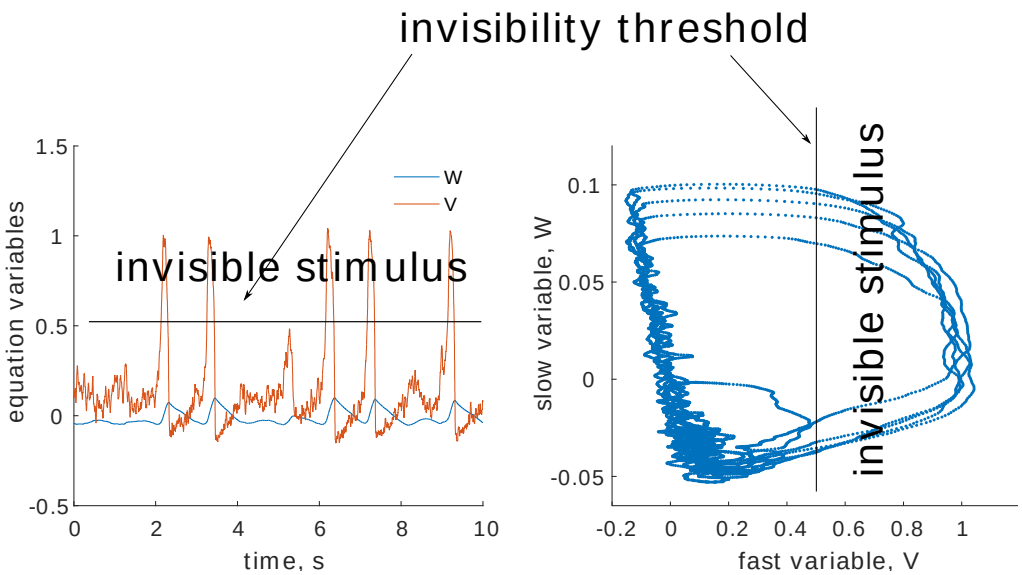

Figure S *2* Illustration of the possible dynamics of the Fitzhugh-Nagumo model describing the Troxler effect. The left plot shows the temporal dynamics of the fast and slow variables, where we assume that the fast variable is responsible for the perceptual visibility of the target. When the fast variable exceeds the threshold denoted by the black line and enters the gray area, the target is perceived as invisible, whereas when it returns to the unshaded region, the target is perceived as visible. The right plot shows the phase portrait of the dynamics showing the points (V(t), W(t)) along the trajectory. The shaded area represents part of the phase diagram where the target is invisible. It can be seen that most of the time the system is near the fixation point, with noise inducing some large trajectories.